Solar Variability: The Connection Between Solar Surface Magnetic flux Density and Solar UV variability

By

Mbonteh Roland Ndunge

A thesis Submitted to the Department of Physics Addis Ababa University In Partial Fulfillment of the Requirements for the Degree of Masters of Science in Astronomy and Astrophysics

Addis Ababa University
College of Natural and Computational Sciences
Department of Physics
Addis Ababa, Ethiopia
July 30, 2024

ADDIS ABABA UNIVERSITY

Author: Mbonteh Roland Ndunge

Degree: MSc

Convocation: July 30, 2024

Addis Ababa University is hereby granted permission to have copies and circulate this research upon the request of individuals or institutions, for noncommercial purposes, and publication(s) of material(s) with findings in this research is reserved to the author.

Author's signature:—————————— July 30, 2024

Addis Ababa University

Department of Physics

The undersigned hereby certify that they have read, understood and recommend to the Faculty of Graduate Studies, for acceptance of the research titled: "Solar Variability: The Connection Between Solar Surface Magnetic flux Density and Solar UV variability" in partial fulfilment of the requirements for the degree of Masters in Astronomy and Astrophysics.

By

Mbonteh Roland Ndunge

Approved by the Examination Committee

Chairman: Signature:——————-Date:——————

Prof. Fekadu Gashaw

Examiner 1: Signature:—————Date:——————-

Examiner 2: Signature:——————Date:——————-

Advisor: Signature:——————-Date:——————-

Dr. Negessa Tilahun Shukure

APPROVAL APPROVAL APPROVAL

Acknowledgement

I would like to sincerely appreciate the following people who have helped me undertake this research:

My supervisor, Dr. Negessa Tilahun Shukure, for his guidance, inputs and enthusiasm for this project, for the sacrifices he made in providing me with necessary tools and materials to undertake this project, for his time and skills for this successful project.

My coordinator, Dr. Teshome Senbeta Debela, for his relentless time and encouragement, for his advises and helpful suggestions, for his selfless efforts in my MS.c career and for his help in facilitating all the administrative duties for my success.

I express my heartfelt gratitude to the entire department of Physics, College of Natural and Computational Sciences, Addis Ababa University.

My sincere gratitude also goes to Dr. Fulvio Franchi and his team for their support.

My special thanks goes to PAPSSN, that gave me the opportunity to study this MS.c program.

I heartily thank my family who set me off on this journey to pursue this MS.c program and I thank the Almighty Father for his countless blessings and protection.

Contents

List of Figures

List of Tables

List of Abbreviations

SOHO	Solar and Heliospheric Observatory
CMs	Coronal Mass Ejections
SUMER	Solar UV Measurement of Emitted Radiation
EUV	Extreme Ultraviolet
SDO	Solar Dynamic Observatory
SORCE	Solar Radiation and Climate Experiment
HMI	Heliosesmic and Magnetic Imager
G2V	G-type-2 main-sequence
UV	ultaviolet
NASA	National Aeronautics and Space Administration
ISS	International Space Station
CN	carbon–nitrogen
CNO	carbon–nitrogen–oxygen
AU	Astronomical Unit
EMI	electromagnetic interference
TV	television
SEPs	solar energetic particles
HR	Hertzsprung–Russell
MH	millionths of solar hemisphere
H	Hydrogen
He	Helium
O	Oxygen
Na	Sodium
Mg	Magnesium
Si	Silicon

Fe	Iron
ECV	Essential Climate Variable
ESA	European Space Agency
TSI	Total Solar Irradiance
SSI	Spectral Solar Irradiance
UVC	Ultraviolet C
UVB	short-wave ultraviolet B
UVA	Long-wave ultraviolet A
PAPSSN	PanAfrican Planetary and Space Science Network
SDO	Solar Dynamic Observatory
SC	Solar Cycle
SOLSTICE	Solar Stellar Irradiance Comparison Experiment
SORCE	Solar Radiation and Climate Experiment
UARS	Upper Atmospheric Research Satellite
GES DISC	Goddard Earth Sciences Data and Information Services Center
XWT	Cross Wavelet Transform
CWT	Continuous Wavelet Transform
WFD	Weak Field Density
COI	Cone of Influence
CI	Confidence Interval
RHS	Right-Hand side
LHS	Left-Hand Side
MUV	mid-ultraviolet
FUV	Far ultraviolet

Dedication

I dedicate this piece of work to my single mother Madam Mbonteh Mary, who has kept me moving forward at all times and set me on this journey early on in life. Her endless encouragement and good upbringing serve as the basis of my successful career.

Abstract

The strength of Solar surface magnetic flux plays an important role in the variability of solar UV irradiance. Several proxies of magnetic activity such as MgII, CaII, and f10.7 have been introduced to correlate solar UV irradiance variability. Daily weak flux densities (WFDs) during solar minimum in 2010 and solar maximum in 2014 calculated from the Solar Dynamic Observatory/Helioseismic Magnetic Imager was used. SSI measurements are from the Solar Stellar Irradiance Comparison Experiment (SOLSTICE). The influence of the magnetic flux density variation on the SSI has been characterized using Spearman, Pearson, and wavelet analysis. The Pear- son's correlation shows that the SSI has a significant positive correlation with weak flux density (WFD) in 2010 and less in 2014; Spearman shows the same. Wavelet analysis also supports the idea that the WFD and SSI have a moderate causality linkage (in both 2010 and 2014) and that the WFD influences solar UV variability on the rotational timescale. The CWT also shows a significant correlation in 2010 than in 2014, while correlogram analysis follows suit and shows more sensitivity between SSI and CaII K lines, indicating a potential shift in solar activity mechanisms and signifying that other external factors are affecting solar activity.

Chapter 1

General Introduction

1.1 The Sun

The Sun is a massive hot ball of plasma or glowing gases (hydrogen and helium), a yellow dwarf G2V star inflated and heated by nuclear fusion reactions at its core at the center of our solar system. The Sun was formed bout 4.6 billion years ago (Bonanno et al., 2002) from a solar nebula (a cloud made up of gas and dust) which collapsed due to strong gravitational attraction, the collapsing cloud started spinning and suddenly flattened into a disk-like structure. At the center of the disk, materials clumped together and became too hot, initiating a nuclear fusion reaction to form a protostar (a ball of hydrogen and helium) that eventually became the Sun, joining other stars in the Milky Way Galaxy whereas the entire flattened disk became the solar system. The Sun is an average star and it is the most important star to us in the entire universe because it is the closest and the only star in our planetary system, all living things on Earth depend on the Sun as a source of energy to permit and sustain life processes as the Sun provides nearly all of our energy on Earth. Some of the Sun's internal energy is emitted from the Sun's surface as light, infrared and UV radiation, providing almost all of the energy for life on our planet. As the nearest star in our planetary system, we can closely study its atmosphere, composition, solar parameters (mass, radius, surface gravity, effective surface temperature etc), structure and several other physical and chemical characteristics in greater details. And information obtained from the studies can be used to test the theories of stellar structure and evolution. We can then improve our theories and have a better understanding of other stars in the universe. The Sun is known to be the largest object in our solar system (Moldwin, 2000).

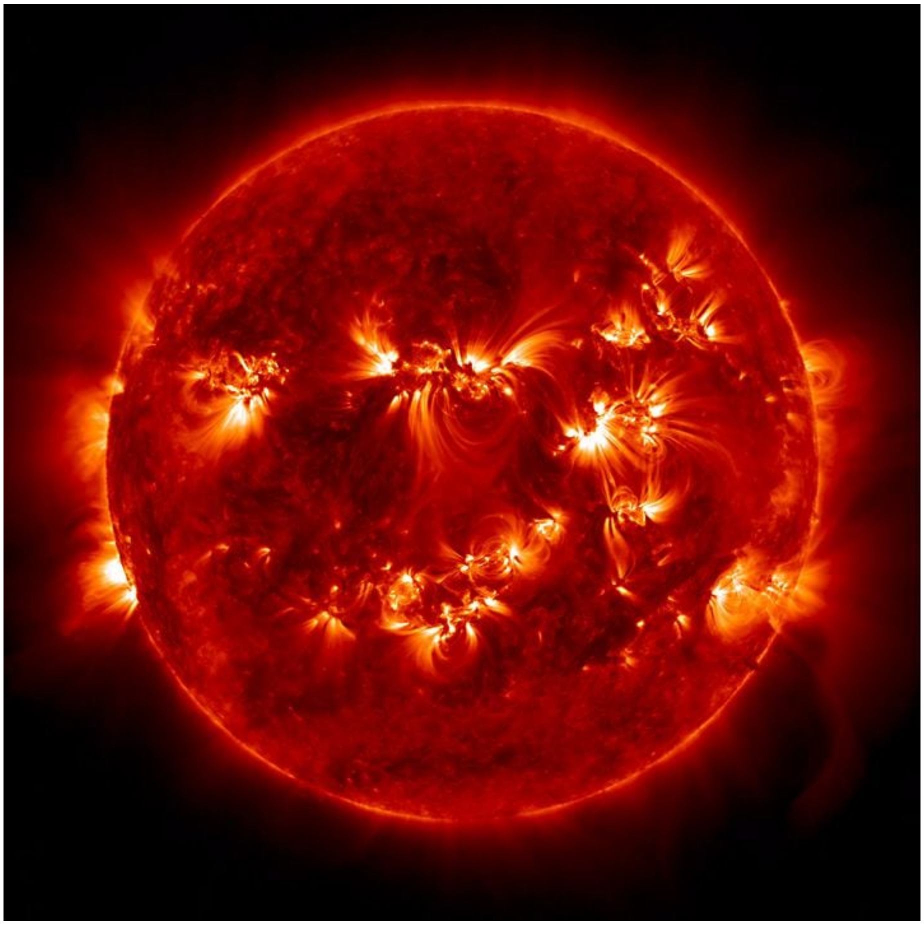

Figure 1.1: The Sun, with active regions. This image was captured in May 2015. The extreme ultraviolet image was taken with the NASA Solar Dynamics Observatory.

A critical component of the Sun is its strong and dynamic magnetic field that causes solar activity, which is a term used to refer to various effects such as sunspots, solar flares and the solar wind. The solar wind is an outward flow of plasma and energetic particles from the Sun which travel through space and has a direct effect on the Earth when these particles collide with our own planetary magnetic field. When these energetic particles are close to the Earth, they are directed into our atmosphere at the poles, as this is where the magnetic field of the Earth originates from. When the particles collide with atoms of oxygen or nitrogen high in the atmosphere the atoms are ionised or electrons in the atoms are excited. When the atoms regain their electrons or the excited electrons drop to a lower energy level again, light is emitted and depending on the reaction involved, we see green, blue or red light. These types of aurora are seen most of the year round but only a few degree from the magnetic poles of the Earth. However, aurora can be seen at more temperate latitudes during a magnetic storm. These are generally caused by CMEs from the Sun that are directed at Earth and the effect is far more pronounced if the magnetic polarisation of the incoming material is southwards. The southward fields cause magnetic reconnection on the day-side of the Earth's magneto-pause which allows the magnetic fields to be dragged over to the night-side of the Earth, where a build up of flux occurs in the magneto-tail. This then reconnects leading to particle acceleration and aurora on the night-side of the Earth

Figure 1.2: ESA astronaut Alexander Gerst took this image of an aurora as he circled Earth on the ISS. Attribution: ESA, and licensed under the Creative Commons Attribution-ShareAlike 3.0 IGO license

1.1.1 Size and Distance of the Sun

The symbol $\odot$, is the astronomical symbol of the Sun used for units such as solar mass $M_\odot$, solar radius $R_\odot$, and solar luminosity $L_\odot$. The radius of the Sun is estimated to be at least 696,342 kilometers (Robitaille, 2013), meaning it will take about 1.3 million Earths to fill the volume of the Sun, while the mass of the Sun is about $1.989x10^{30}$kg, meaning it will take at least 330,000 Earths to match the Sun's mass (Woolfson, 2000). The Sun is about 150 million kilometers (AU) from Earth. Its nearest stellar neighbor is the Alpha Centauri (a triple star system consisting of: red dwarf star Proxima Centauri which is about 4.2 light-years away (Fraknoi et al., 2018), followed by Alpha Centauri A and B, two sun-like stars orbiting each other about 4.4 light years away (Fraknoi et al., 2018).

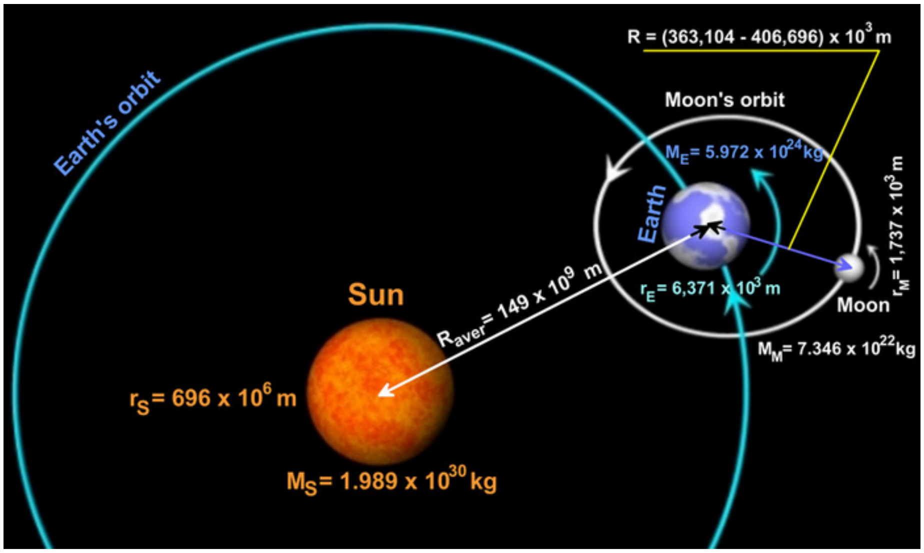

Figure 1.3: Simplified scheme (not to scale) of the Sun-Moon-Earth interaction with their masses (M) and distances (R) between the Sun and the Earth and Moon and Earth and radii (r). The subscripts S, E and M denote the Sun, the Earth and the Moon, respectively (Arsen'yev et al., 2019). This image is credited to Eppelbaum (2019).

1.1.2 Orbit and Rotation of the Sun

The Sun is orbiting the center of the Milky Way galaxy and it's located in the spiral arm of the Milky Way galaxy called the Orion Spur which extends outward from the Sagittarius arm. The Sun orbits the Milky Way galaxy together with our entire solar system including planets, comets, asteroids, and all other objects in our solar system. Our solar system moves with an average velocity of about 720,000 kilometers per hour, yet it still takes about 230 million Earth years for the Sun to make one complete revolution around the Milky Way galaxy. The Sun is also rotating on its axis as it revolves around the Milky Way galaxy. The Sun spin has a tilt of about 7.25 degrees with respect to the plane of it's planets' orbits. Different parts of the Sun rotate at different rates because the Sun is not solid. For example, at the Sun's equator, the Sun spins around once roughly every 25 Earth days while at the Sun's poles, it rotates around once on its axis every 36 Earth days.

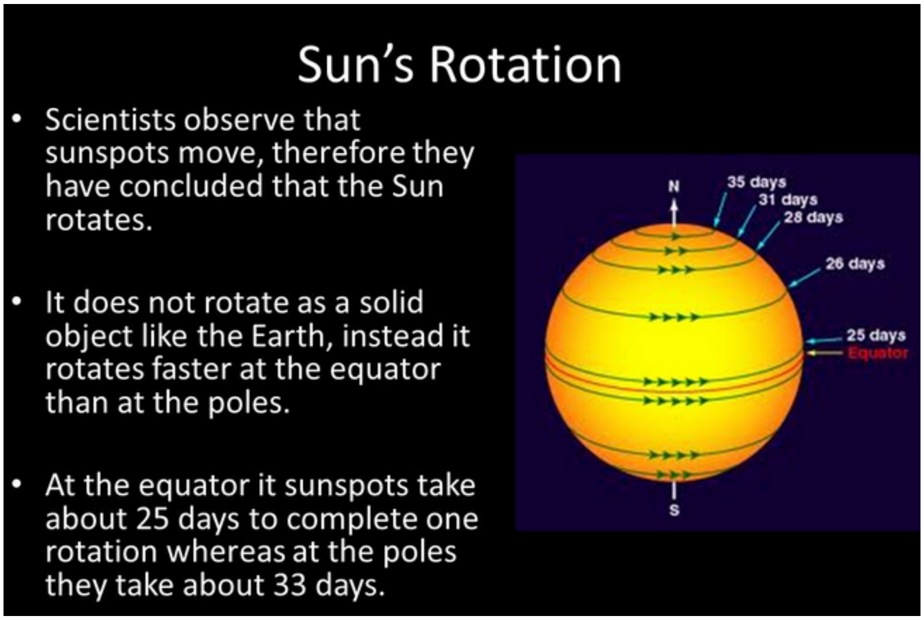

Figure 1.4: This image shows the rotation of the Sun and how it differs by latitude. Earlier studies revealed the Solar surface rotation (Thompson et al., 2003). (Image credit: NASA)

1.2 The Structure of the Sun

The Sun's chemical composition is thought to be practically homogeneous from its center to its surface. But from the point of view, the sphere of the Sun consists of different layers, each of which plays a different role in the transfer or production of energy. Some layers of the Sun have been regularly observed directly for a very long period while other layers have been studied either theoretically (i.e the Sun's core and its convective zone) or occasionally (i.e the corona, e.g during solar eclipses). In new methods of observations, both ground-based and space-based instruments are being used with remote sensing or in situ measurements to obtain new and more accurate information about each of the layers of the Sun. From the deep core of the Sun to the distant rarefied corona and even the solar wind, plasma and magnetic fields penetrate far into our solar system.

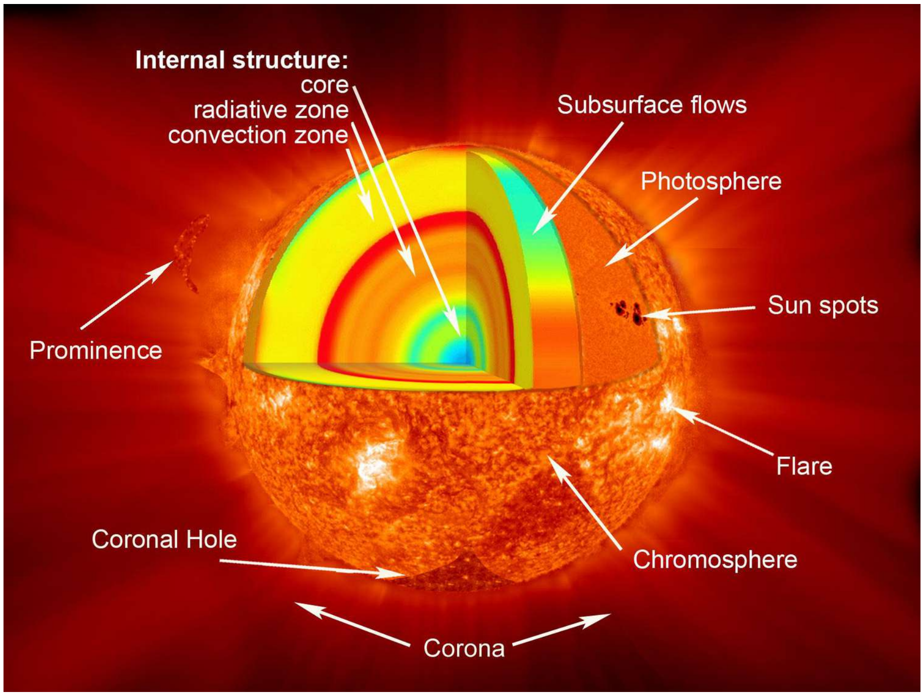

Figure 1.5: This illustration shows the different parts of the Sun, from the hot core where the energy is generated through regions where energy is transported outward, first by radiation, then by convection, and then out through the solar atmosphere. The parts of the atmosphere are also labeled the photosphere, chromosphere, and corona. Some typical features in the atmosphere are shown, such as coronal holes and prominences (Lkhagvadorj, 2023)

.

1.2.1 The Core of the Sun

The Sun's core extends from its center to approximately 20-25 percent of the solar radius (García et al., 2007), with a density of 150g/cm (roughly 150 times the density of water) (Basu et al., 2009), with a temperature of about 15.7 million Kelvin (K) (Howe, 2009). In the Sun's core, energy has mostly been produced by nuclear fusion through a proton-proton (p-p) chain (a set of nuclear reaction in which hydrogen is converted into helium) while the other set of fusion reaction in which hydrogen is converted into helium is the CNO Cycle, which currently generates about 0.8 percent of the Sun's energy (Imbriani et al., 2004). The core of the Sun is the only region of the Sun that produces an enormous amount of thermal energy through nuclear fusion.

1.2.2 Radiative Zone

The Sun's radiative zone is the thickness layer of the Sun (at about 0.45 solar radii). The radiative zone is the layer just outside of the core of the Sun. In this layer, photons of light carry energy created through nuclear fusion reactions in the core of the Sun towards the surface as thermal radiation. It can take several millions of years for the energy to travel through this radiative zone. Density and temperature decrease as you further away from the core of the Sun, such that near the top of the radiative zone, temperatures cool to about 2 million ℃. The radiative zone is the transition zone between the core and the convective zone, and it extends about two-third away to the solar surface.

1.2.3 The Convective Zone

The convective zone of the Sun extends from about 0.7 solar radii (500,000km) to near the surface of the Sun. The outermost region of the Sun's interior is called the convective zone. This zone extends from the radiative zone to the solar surface. Within this zone, the expanding hot plasma of the Sun carries energy upward, to the Sun's surface. The plasma cools as it moves upward, dropping to about 5,700 ℃ at the top of the convective zone. As the temperature cools, the plasma becomes denser and sinks towards the bottom of the convective zone. At this point, the temperature rise again from deeper within the Sun and rises towards the solar surface. Energy flows through these convection currents, and appears as granules on the visible solar surface.

The radiative and the convective zone of the Sun are separated by a transition layer called the tachocline.

1.2.4 The Photosphere

Unlike Earth, Moons or other rocky planets, the Sun does not have a solid surface. The photosphere is the portion of the Sun commonly referred to as its surface. The photosphere is the visible or the first layer of the nonuniform surface of the Sun. The thickness of the photosphere is roughly 250 miles, and its temperatures reach closely to 10,000 degrees Fahrenheit or 5,500 degrees Celsius. Most of the radiation of the Sun escapes outward from the photosphere into space. Above the Sun's photosphere is the chromosphere, the transition zone, the corona and the heliosphere which all make up the atmosphere of the Sun. We note that the Sunlight at the top of the atmosphere of the Earth is made up of about 50 percent infrared light, 40 percent visible light, and about 10 percent UV light. The Earth atmosphere filters out more than 70 percent of the Sun's UV, mostly at shorter wavelengths. The Solar UV ionizes our Earth's day-side upper atmosphere, hence creating the electrically conducting ionosphere which UV light from the Sun has some antiseptic properties used to sanitize water. Solar UV also causes Sunburns and has other uses as the production of vitamin D and Sun tanning. Solar UV is also the main cause of diseases like skin cancer. Solar UV light is highly attenuated by the ozone layer of the Earth, hence the amount of the Solar UV entering the Earth varies greatly with latitude and this is also responsible for several biological adaptations like variations in the color of humans in different areas of the Earth.

Solar Activity Features on the Photosphere

Sunspots

Sunspots can be seen as dark patches on the photosphere of the Sun and they correspond to concentrations of magnetic fields where the convective transport of thermal energy is inhibited from the solar interior to the solar surface. Due to this, sunspots are less cooler than the surrounding photosphere, making them to appear dark. Few sunspots are visible, and sometimes none can be seen at all. The sunspots that appear are at high solar latitudes. As the solar cycle approaches its maximum sunspots tend to form closer to the solar equator, a process known as the Sporer's law. The biggest sunspots can be tens of thousands of miles across.

Faculae

Faculae refer to the bright areas that are usually observed near the limb, or edge, of the Sun's disk. These are also magnetic areas though the magnetic field is concentrated in smaller bundles than in sunspots. While the sunspots make the Sun look darker, faculae make the Sun look brighter. During a sunspot cycle, faculae win out over sunspots and make the Sun appear slightly (about 0.1%) brighter at sunspot maximum than at sunspot minimum.

Photospheric Network

Various spectroheliograms obtained by Chapman and Sheeley Jr (1968) in some of the Fraunhofer lines with an 82-cm solar image at Kitt Peak National Observatory, showed a bright photospheric network, with the following properties:

(1) The network resembles, and does not coincide with chromospheric network, the structure of the photospheric network is finer and more delicate than the relatively coarse structure of the chromospheric network.

(2) The network is exactly cospatial with the network of non-sunspot photospheric magnetic fields.

(3) The visibility of the network in a given photospheric Fraunhofer line is primarily dependent on the states of the ionization and excitation from which the line is formed, and secondarily dependent on the Zee-man sensitivity of the line, being most visible in low-excitation lines of neutral atoms, and least visible in high excitation lines of singly ionized atoms.

These magnetic regions of the solar atmosphere are a few hundred degrees hotter than their surroundings, and they are visible in white light near the limb as photospheric faculae (Chapman and Sheeley Jr, 1968).

Granules

Granules refer to small (about 1000 km across) cellular features covering the entire Sun, except those areas covered by sunspots. The features are the tops of convection cells, where hot fluids rise up from the Sun's interior in the bright areas, spreads out across the surface then cools and suddenly sinks inward along the dark lanes. Individual granules last about 20 minutes.

Supergranules

Supergranules are larger versions of granules (about 35,000 km across) but are mostly seen in measurements of the "Doppler shift" where light from materials moving toward us are shifted to the blue while light from materials moving away from us is shifted to the red. The features also cover the entire Sun and they are continually evolving. Individual supergranules last about a day or two and they have flow speeds of about 0.5 km/s. The fluid flows observed in supergranules carry magnetic field bundles to the edges of the cells where they then produce the chromospheric network.

1.2.5 The Chromosphere

The chromosphere of the Sun is the layer above the solar photosphere. With a very low density, it is impossible to observe the chromosphere during a total solar eclipse, due to its brightness. The chromosphere is less dense than the photosphere.

Solar Activity Features on the Chromosphere

Filaments and Plage

Filaments refer to dark, thread-like features observed in the red light of hydrogen (H-α). They are dense, cooler, clouds of material suspended above the surface of the Sun by loops of magnetic fields. Plage are also associated with concentrations of magnetic fields and form a part of the network of bright emissions that characterize the solar chromosphere.

Spicules

Spicules refer to small, jet-like eruptions observed throughout the chromospheric network. They last just a few minutes and in the process, they eject material off of the solar surface and outward into the hot corona at a speeds of about 20 to 30 km/s.

The Chromospheric Network

Chromospheric network refers to a web-like pattern mostly observed in the emissions of the red line of hydrogen (H-α) and the ultraviolet line of calcium (Ca

II K - from calcium atoms with one electron removed). This network outlines the supergranule cells due to the presence of bundles of magnetic field lines concentrated in the supergranules.

The Flares

Solar flares also indicates solar activity. Materials are usually ejected from its chromosphere and corona of the Sun. The materials contain a large amount of energy released by the Sun, in the form of flares. The flares are usually observed from Earth as a flash of light that increase the brightness of the Sun. At times, the flares are extremely powerful and the materials ejected (like electrons and hydrogen atoms) escape from the Sun´s gravitational field so that they are free to travel throughout the Solar System.

Solar Chromospheric Activity

The chromosphere exhibits a range of phenomena collectively called activity (Hall, 2008). Thes activities can be studied using proxies like CaII K lines and MagII index.

1.2.6 The Corona

The corona is the biggest and the least dense structure of the Sun. The corona is composed of plasma escaping from the Sun that reaches about 1.000.000 kelvin, but with a density lower than that of the chromosphere. Moreover, the solar wind transports the material of the corona out to the interplanetary space.

Solar Activity Features on the Corona

The Prominences

Prominences are also called filaments, they are formed in the corona. A prominence is a large structure of gas at a high temperature that is held up by magnetic field lines above the solar surface.

The Coronal Mass Ejections

CME may occur due to twisted magnetic field holding up a prominence becomes unstable, rises up and quickly. If this happens, the materials of the prominence get released out of the Sun, and reaches a speed of about 1000 km/s. This is known as a CME. Sometimes this happen at the same time with solar flares, but the flares release light, while a coronal mass ejection releases material.

Solar radio flux at 10.7 cm (2800 MHz) is an indicator of solar activity. Also called the F10.7 index, it's one of the longest records of solar activity. F10.7 radio emissions originates high in the chromosphere and low in the corona of the Sun's atmosphere.

Some properties of the Sun:

Characteristic	**Value**
Mass	1.989×10^{30} kg
Radius	6.9599×10^{5} km
Mean density	1.409×10^{3} kg·m^{-3}
Core density	1.48×10^{5} kg·m^{-3}
Luminosity	3.86×10^{26} W
Effective temperature	5780K
Core temperature	15.6×10^{6} K
Age	4.6×10^{9} y
Rotation period	25–35d
Magnetic field	0.1–0.4 T
Escape velocity (at photosphere)	6.177×10^{2} km·s^{-1}
Free fall acceleration at surface	2.74×10^{2} m·s^{-2}
Chemical composition (number of atoms)	91% H, 9% He, 0.1% other
Chemical composition (mass)	71% H, 27% He, 2% other
In relation to the Earth	
Mean distance	1.496×10^{8} km
Minimal distance (∼January 3)	1.471×10^{8} km
Maximal distance (∼July 7)	1.521×10^{8} km
Angular size (at mean distance)	31.99°
-	-

Table 1.1: Characteristics of the Sun

	Location	**Thickness**	**T**	**p**	**n**
	(km)	(km)	(K)	(kg m^{-3})	(particles m^{-3})
Core	0–5×10^{5}	5×10^{5}	15.6×10^{6}	1.48×10^{5}	—
Convection zone	5–7×10^{5}	2×10^{5}	10^{6}	10^{1}	—
Photosphere	—	300	6×10^{3}	2×10^{-4}	10^{11}
Chromosphere	—	1500	10^{4}	3×10^{-9}	10^{7}
Inner corona	—	100000	1.5×10^{6}	10^{-12}	3×10^{3}
—	—	—	—	—	—
—	—	—	—	—	—

Table 1.2: Parameters of the Sun's primary layers

1.3 The Sun as a Main-sequence Star

When the Sun reaches its main sequence in an HR diagram, the luminosity of the Sun is ensured by its vast nucleus supply of hydrogen continuously converting into helium during the proton–proton cycle at its core. Stars which are more massive than the Sun have greater temperatures in their cores due to greater hydrogen conversion in to helium. If the temperatures at the core are higher than $16x10^6$K, several types of nuclear fusion occur, like the CN cycle. These mechanisms are more effective, though the available supply of hydrogen is spent in a more shorter period of time. According to some realistic estimations by scientists, it will be around $5x10^9$y before the Sun completely depletes the vast amount of usable hydrogen in its core at its present consumption rate. The rate of nuclear fusion in the Sun's core is self-regulated by a balance between the radiation pressure and the gravitational pressure due to the higher levels of solar mass being attracted. The Sun will be within its main sequence up to about twice its present age. The uncertainty in the estimated time is because of the doubts about the exact amount of helium in the protosun, some estimates of which range between 24-28 percent by mass. Therefore, the higher the helium content, the lesser the hydrogen is to be converted into helium before the Sun moves out of its main sequence.

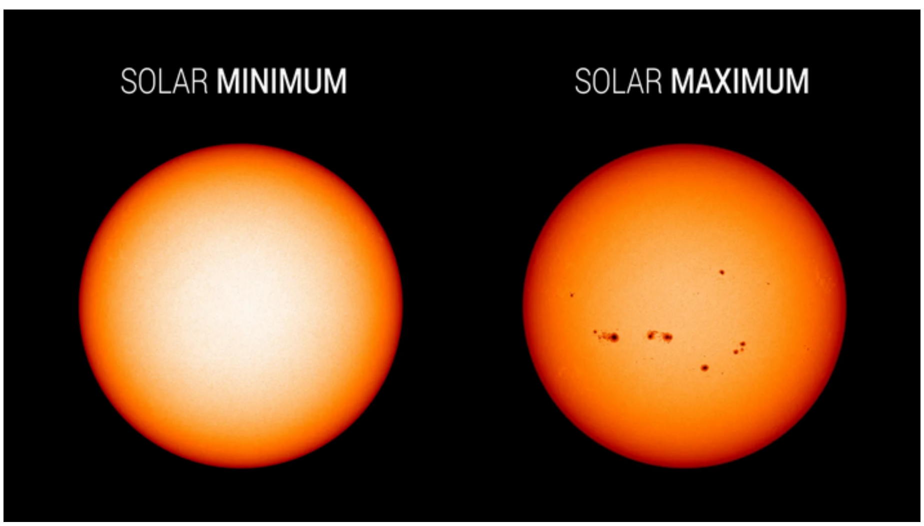

Figure 1.6: Visible-light images from NASA's Solar Dynamics Observatory show the Sun at solar minimum in December 2019 and the last solar maximum in April 2014. Sunspots freckle the Sun during solar maximum; the dark spots are associated with solar activity. Credits: NASA's Solar Dynamics Observatory/Joy Ng

1.4 Solar Indices

1.4.1 Sunspot Area and Sunspot Number

Sunspots are associated with intense magnetic fields (Hayakawa et al., 2024) and they vary in size, in shape, and in complexity. These intense magnetic activity inhibit convection and reduce the surface temperature on regions of the solar surface (photosphere), forming dark spots called Sunspots. The measure of the size or extent of the sunspots on the solar surface is known as Sunspot area. The measurement unit of sunspot area is PPM, solar telescopes equipped with filters to observe and measure sunspot areas accurately are used for measuring sunspot area. Sunspot area can be used to illustrate the development of sunspot groups (Balmaceda et al., 2009). Sunspot area has close similarity to the solar activity cycle, which has an 11-year periodicity. During periods of high solar activity (or solar maximum), sunspots area become larger and numerous sunspots are observed. While during periods of low solar activity (or solar minimum), sunspot areas decrease, and less sunspots are seen. Sunspot areas can change over time this is because individual sunspots can either grow, merge, or decay, therefore affecting the overall sunspot area. This evolution of sunspot areas can provide significant insights into the development of solar magnetic structures, the progression of the solar cycle and the emergence of new active regions. Large sunspots with bigger areas are mostly associated with solar flares, which are explosive releases of energy and radiation from the Sun. The strong magnetic fields within sunspots can lead to magnetic reconnection events, thereby triggering flares and energetic particle emissions on the solar surface. Measurement of sunspot area is essential for space weather forecasting. Solar flares, CMEs, and energetic particle events related with sunspots can impact the Earth's atmosphere, and technological systems such as power grids satellites and communication networks.

While sunspot number is an important metric used in solar physics to quantify the level of solar activity based on the number of sunspots visible on the solar surface. Sunspot number is a crucial indicator of solar activity and magnetic variability. Sunspot number reflects the presence and the intensity of magnetic disturbances on the Sun's photosphere, which are associated with phenomena like geomagnetic storms, solar flares and CMEs. Sunspot number vary from day to day and over the course of the entire solar cycle. Long term trends in the sunspot number indicate patterns of solar variability, including the occurrence of solar maxima and solar minima. Understanding these variations help us understand the dynamics of the solar magnetic field and its implications on space weather.

MgII, CaII K lines, and F10.9 are other examples of solar indices, these are well discussed in chapter 2.

1.5 Solar Surface Magnetic flux

The presence of magnetic fields causes the Sun to depart from spherical symmetry. These magnetic fields give rise to a variety of observational phenomena. The magnetic activity is used to cover the magnetically driven phenomena which are some times a striking characteristic of the Sun. Under magnetic activity, we include the presence of faculae, sunspots, prominences, and the chromospheric network, all of which are more or less long-lived phenomena, which can naturally be regarded as quasi-stationary. On the other hand, magnetic activity also includes phenomena which are not also stationary, such as flares and CMEs. Both of the latter involve highly time dependent processes which disturb the solar atmosphere sometimes by giving rise to fireworks displays which involve the most energetic phenomena in the solar system. The magnetic fields on the Sun's surface are believed to be generated by dynamo action driven by convective motions below the surface of the Sun (Ghizaru et al., 2010). Many important dynamo processes take place below the solar surface, where the details are still to be well understood, since the tools readily available for probing the subsurface dynamics of the magnetic fields are theory and helioseismology and both have unveiled some of the dynamics (Gizon and Birch, 2005). Humans knowledge of the magnetic field dynamics at the surface of the Sun can be inferred from high resolution spectropolarimetric observations, e.g, the Hinode spacecraft with about 230 km resolution (Tsuneta et al., 2008) and the Sunrise balloon-borne solar observatory with about 100 km resolution (Solanki et al., 2010). The magnetic field at the Sun's surface is observed to be structured on all spatial scales (Solanki et al., 2006).

1.5.1 Mechanism of formation of solar surface magnetic flux

Several observations indicate that magnetic fields originate into the Sun's photosphere as bundles of magnetic flux (or magnetic flux tubes) according to (Cheung, 2006). The mechanism of formation of solar surface magnetic flux corresponds to the emergence leading to the establishment of magnetized structures in the solar atmosphere (Schmieder and Pariat, 2007). The solar surface magnetic flux is directly traced on the Sun's surface in visible white light by the presence of dark sunspots surrounded by plages (brighter regions). Several measurements of magnetic fields on the Sun's surface shows that sunspots are grouped in pairs with a positive and negative magnetic polarity, forming an active region. The occurrence of large-scale magnetic flux emergence turn to follow the solar cycle periodicity which is governed by the process of solar dynamo. The surface of the Sun is also covered by magnetic carpet with relatively small magnetic bipoles which are scattered allover the Sun's surface. The bipoles are as a result of the recycling of magnetic field by convection (granules and supergranules). The emergence of magnetic flux from the solar interior towards the visible solar surface or photosphere and beyond is a key aspect of solar magnetic activity. Due to magnetic buoyancy, the magnetic fields rise towards the surface of the Sun, convective motions (updrafts and downdrafts) giving an impact on the shape of the emerging fields, which develop a serpentine-like configuration over a large range of spatial scales (Archontis and Syntelis, 2019). On small scales (1–2Mm), granular convection affects the formation of magnetic fields, which appear to the photosphere in the form of small magnetic bipoles, while on large scales (100Mm), the interplay between convection, photospheric motions and interaction of the small emerging bipoles (cancellation, coalescence, etc.) lead to the formation of sunspots and active regions. The source of the magnetic field at the coronal region, active regions, sunspots birth, are believed to originate in the interior of the Sun, a place where an invisible dynamo process generates magnetic fields that are transported by magnetic buoyancy to the surface of the Sun, this process that is called "magnetic flux emergence". The review of Cheung and Isobe (2014) discuss the theory of emerging flux, and Fan (2009) discuss the related magnetic fields in the solar convection zone. The buoyancy force which is the main driver of the flux emergence strictly depends on the pressure balance between a magnetic flux tube and the ambient nun-magnetized fluid,

$$p + (B^2)/8\pi = pe \tag{1.1}$$

where $p = internal$ gas pressure in the flux tube, $B = magnetic$ field strength in the flux tube, and $pe = pressure$ of the external fluid. The physical principles of 3-D MHD equations generally used to model emerging flux scenarios includes energy conservation, momentum conservation, mass conservation and Faraday's law of electromagnetic induction (eliminating the electric field),

$$dB/dt = \nabla x(uB) + \eta\nabla^2 B \tag{1.2}$$

where $\eta = Ohmic$ magnetic diffusivity and $u = velocity$ of the plasma motion. The first term on the right-hand side describes changes to the magnetic field as it is advected by plasma flows with the speed u, and the second term on the right-hand describes changes due to magnetic field diffusion. The relative importance of these terms is given by the Reynolds number equation

$$Rm = vl/\eta \tag{1.3}$$

where $v = velocity$ and $l = length$ scale. If $Rm >> 1$, the advective term dominates, as in the case for the solar corona, but in the case with dominant diffusion, ($Rm << 1$) is not relevant for typical solar conditions. The diversity of MHD models used in several numerical simulations of flux emergence is divided into three as seen in Cheung and Isobe (2014), which are: (i) idealized models that include energy sources, energy sinks, thermal conduction, convective flows, neutralion effects and magnetic reconnection; (ii) realistic models that additionally include non-local thermodynamic equilibrium effects and radiative transfer (iii) data-driven models that are computed with time-dependent boundary conditions driven by observed real data on scales of the entire active regions. So far, one of the most developed numerical MHD models of flux emergence are known to be provided by Tian et al. (2011), Cheung (2006), Tortosa-Andreu and Moreno-Insertis (2009), Rempel and Cheung (2014), they simulated the phenomenon of flux emergence from the convection zone via the photosphere, chromosphere, and corona. Some earlier simulations of flux emergence began with an insertion of a horizontal flux tube at some depth of the convection zone, which buoyantly rises towards the photosphere, while lateral pressure equilibrium causes a flattening into a horizontally extended sheet-like structure (Mestel and Spruit, 1987) and it is reproduced in recent radiative MHD simulations (Toriumi et al., 2011). During the upward motion of a flux emergence structure, different magnetic buoyancy instabilities kicked in, such as the interchange mode (Kruskal-Schwarzschild instability), or the undular mode (Parker instability). The undular instability of a horizontal magnetic layer is eminent in shaping the formation of the arching flux tubes (Fan, 2009). The interaction of the convective down-flows with the rising magnetic flux tubes undulates the magnetic field to form serpentine field lines that arise into the photosphere (Pariat et al., 2004). The horizontal expansion of a buoyantly rising flux tube can be suppressed in the presence of an ambient magnetic field by the magnetic tension in the azimuthal component of a twisted flux tube (Shibata et al., 1993). The presence of Alfvén waves were found to contribute an important role in the simulation of buoyancy instabilities (Manchester et al., 2006). Depending on the topology of the external flow field, an emerging flux tube can modify the local granulation pattern and lead to the transient appearance of dark lanes (Cheung, 2006).

1.5.2 Strong Week solar surface Magnetic flux

Babcock and Babcock (1955) were the first to write about the distribution of magnetic fields on the surface of the Sun, outside the sunspots . Their magnetograms covered the period within 1952-1954, the last minimum of solar activity by 1965. They showed the existence of Bipolar Magnetic Regions, which are the magnetic fields of active regions. This was well explained by Babcock (1961) as the result of the preferential poleward drift of the portions of BMR's. The daily magnetograms obtained since 1959 gave a much improved picture of the solar magnetic field distribution, and for this reason it was very appropriate to examine the material in detail for a study of the large-scale distribution of magnetic fields on the surface of the Sun. Today, there is much available information about two distinct components of magnetic fields in the Sun. One is the global and quite weak, while the other is highly localized and extremely strong, mostly in the sunspots. The localized fields are stronger than the global and quite weak fields by factors of at least 100 to almost 1000. In the sunspot's umbra, the direction of the field is found to be vertical (perpendicular to the solar surface). As we move from the umbra outward into the penumbra, the field lines are seen to be tilted more and more toward to a horizontal direction: the horizontal fields give rise to dark and bright striations or zebra-stripes which are the hallmark of the penumbra when observed at high angular resolution. The field is highly clumped into compact flux ropes. At the center of each flux rope, the field may reach values of about 1–2 kG. This results to the graphic term "pin-cushion" which is at times used to describe the nature of the magnetic field structure in the quiet Sun. Given a field of view of an instrument, the average magnetic field strength that could be measured for that particular area depends on how many magnetic pins lie within the field of view. Active regions are mainly the locations where there are enhanced areal densities of the magnetic pins while sunspot umbrae are locations where the areal density of magnetic pins reaches a maximum.

1.5.3 Week solar surface Magnetic flux

Babcock and Babcock (1955) also showed the Unipolar Magnetic Regions, which are the extended weak regions of one polarity. The polar field was also observed to reverse polarity according to Babcock (1959) at the time of activity maximum. The active regions surrounding the sunspots have fields of hundreds of G. In the quiet Sun, the average magnetic fields (averaged over a field of view of, say, 10 $arcsec^2$) are weaker, and are not uniformly distributed. Solanki et al. (2006) describes the magnetic field as it threads from the bottom of the convection zone of the Sun, where it's built up by the solar dynamo, to the surface of the Sun.

1.6 Statement of the Problem

The magnetic field of the sun extends throughout its entirety, encompassing the entire solar system. The solar activity is thought to be the responsible driver of the solar UV irradiance variability. However, the magnetic flux density on the solar surface assumed to have an influence on the variability of UV radiation. However, further investigation is required to thoroughly understand this relationship. This thesis aims to investigate the relationship between solar surface magnetic flux density and solar UV variability by employing a variety of techniques.

1.7 Research Question

The following research questions are answered in this thesis:
a) How is solar UV variability influenced by solar surface magnetic flux density?
b) What are the effects of solar UV irradiance on Earth's climate and environment?

1.8 Objectives of the Study

1.8.1 General Objective

The general objective of this study is to investigate the connection between solar surface magnetic flux density and solar UV variability.

1.8.2 Specific Objectives

The specific objectives of this project are as follows:
a) To characterize the influence of solar surface flux density on solar UV variability during solar minimum (in 2010) and solar maximum (in 2014).
b) To Study the casualty linkage between solar UV variability and solar surface magnetic flux density during the solar minimum in 2010 and solar maximum in 2014.

1.9 Strengths and Limitations

This project fall-short of the study of solar interior, thereby focusing on regions of weak magnetic fields. It covers the influence of magnetic features (such as solar activity) from the photosphere of the sun to its corona and possibly its effects on our planet. This project focuses mainly on the UV spectrum of the sun and its variability, as influenced by solar surface magnetic flux density.

Chapter 2

Literature Review

2.1 Magnetic Fields and UV Emission

The solar surface magnetic fields can influence the behavior of solar UV emissions (Erdmann et al., 2021), in active regions like solar flares and weak active regions. During solar events, increased UV radiations can be caused by strong magnetic fields by trapping and accelerating charge particles. Due to the significant importance of solar surface magnetic filed and solar UV irradiance with profound effects on the Earth's atmosphere, weather and climate, solar astrophysicists have been stimulated to understand the nature of solar UV irradiance and it effects on our climate.

Over many decades, numerous space-based measurements, calculations and modeling techniques have been employed to study these phenomena. Up to now, there isn't a sufficient understanding, accuracy and regularity to conclude the nature of the relationship between solar UV variability and the strength of magnetic flux on the Sun's surface.

To study this relationship, researchers have used proxies like He I 584 Å (Pauluhn and Solanki, 2003), using data collected by the SUMER spectrograph on SOHO. They found that solar UV variation is due to changes in solar magnetic network. Fligge et al. (2000) presented the first model to make direct use of magnetic maps (together with calculated intensity spectra) to reconstruct irradiance and strengthens on the hypothesis that magnetic field is the dominant driver of solar UV irradiation variations. According to (Solanki et al., 2013), the main drivers of solar variability are thought to be magnetic features at the solar surface. According to Domingo et al. (2009), Phenomenological models of the solar atmosphere in combination with imaging observations of solar electromagnetic radiation and measurements of the photospheric magnetic field have reached high enough quality to show that a large fraction (at least, about 80%) of the solar irradiance variability can be explained by the radiative effects of the magnetic activity present in the photosphere. Other proxies found in chromospheric layers such as Ca K, Mg II and other parameters have been used to study the effects of solar UV variability.

These findings have given us ideas that there can be an interaction between magnetic fields and UV but fall short of explaining how magnetic fields influences UV on the solar surface.

2.2 History of observation of the Sun

Solar observation refers to the scientific endeavor of studying the Sun, its behavior and its relation to the Earth and the rest of our Solar system. The Sun has been an important object of veneration in many cultures around the world throughout human history. Humanity's fundamental understanding of the Sun is as the luminous disk in our sky, whose presence and absence causes day and night respectively. In many ancient and prehistoric cultures, the Sun was believed to be a solar deity, a supernatural god or other mysterious entity. The Sun has also played a very important rule in many world religions. Since in the first early millennium BC, the Babylonian astronomers observed that the Sun's motion is not uniform along the ecliptic, but they didn't know why. It is known today that it's due to the movement of the Earth in an an elliptic orbit around the Sun, with our Earth moving faster when it is closer to the Sun at perihelion and moving slower around the Sun when it is farther away at aphelion.

It is believed that the Greek philosopher Anaxagoras was one of the first people to offer a philosophical or a scientific explanation of the Sun. It was reported that Anaxagoras reasoned the Sun was not the chariot of Helios and instead a giant flaming ball of metal that is even larger than the land of the Peloponnesus and that the Moon was reflecting the Sun's light. Eratosthenes later estimated the distance between the Earth and the Sun around the third century BC, to be within 148 million kilometers to 153 million kilometers or within 0.99 AU to 1.02 AU. In the third century BC, an ancient Greek, Aristarchus of Samos proposed a theory that the Sun is the center around which the planets orbit and it was later adopted by Seleucus of Seleucia. This theory was then developed in the 16th century by Nicolaus Copernicus in a more detailed mathematical model of a heliocentric system. Around 206 BC to 220 AD, Chinese astronomers recorded observations of sunspots during the Han Dynasty and they maintained the records of these observations for several centuries. In the 12th century, a description of sunspots were also provided by Averroes. Solar observation lead to the invention of telescopes in the early 17th century by Galilei Galileo, Thomas Harriot and other astronomers which permitted detailed observations of sunspots. In 1666, a prism was used by Sir. Isaac Newton to observe the light of the Sun, and he showed that the Sun is made up of light with many colors. William Herschel then discovered infrared radiation beyond the red part of the solar spectrum in 1800. In the 19th century Joseph Von Fraunhofer recorded more than 600 absorption lines in the spectrum which are still considered to be the strongest today, often referred to as the Fraunhofer lines. In the 20th century specialized systems were used for solar observation at different narrow-band wavelengths, such as those using Calcium H (396.9

nm), K (393.37 nm) and hydrogen-alpha (656.46 nm) filtering. In 1904 Ernest Rutherford suggested that the Sun's output could be maintained by an internal radioactive-decay source of heat. Albert Einstein then provided the source of the energy of the Sun, $E = mc^2$. In 1920, Sir. Arthur Eddington suggested that the temperatures and pressures at the Sun's core could produce a nuclear fusion reaction that merged hydrogen (protons) into helium nuclei, which result in the production of energy from the net change in mass. In 1925, Cecilia Payne confirmed the preponderance of hydrogen in the Sun by using the ionization theory developed by Meghnad Saha. In the 1930s, Hans Bethe and Subrahmanyan Chandrasekhar developed the theoretical concept of fusion. The details of the two main energy producing nuclear reactions that power the Sun was calculated by Hans Bethe.

2.2.1 Ground based solar observatories

An observatory is a well designed location used for observing celestial, marine or terrestrial events. Astronomy is the best example of a discipline for which observatories have been well constructed and used. Since from ancient history, observatories were as simple as containing an astronomical sextant (for measuring the distance between stars) or Stonehenge (which has some alignments on astronomical phenomena). Astronomical observatories are divided into four categories namely space-based observatories, airborne observatories, ground-based observatories, and underground-based observatories. Here, we will throw some light on ground-based and space-based observatories. Ground based solar observatories are located or constructed on the surface of Earth, and are used to make observations of the Sun in the radio and visible light portions of the electromagnetic spectrum. Many optical telescopes are housed within a dome or similar structure for protection and blocking of light from the surrounding. Telescope domes have a slit or other openings in the roof that are opened during observing, and closed when the telescope is not used. In most cases, the entire upper portion of the telescope dome can be rotated to allow the instrument to observe different portions of the sky. Ground based Radio telescopes which usually do not have domes can also be used for solar observation within the radio spectrum. For optical telescopes, most ground-based observatories are located far from major centers of population towards darker areas and away from streetlights, to avoid the effects of light pollution. The best locations for modern observatories are sites that have dark skies, a large percentage of clear nights per year, dry air, and are at high elevations such as in most places in Africa. This is because at high elevations, the atmosphere of the Earth is thinner, thereby minimizing the effects of atmospheric turbulence and leading in better astronomical observation. Sites that meet all the mentioned criteria for modern observatories include Africa, Hawaii, the Andes, southwestern United States, Canary Islands, and high mountains in Mexico such as Sierra Negra. Major optical observatories include: Roque de los Muchachos Observatory in Spain, the Mauna Kea Observatory and Kitt Peak National Observatory in the US, the Paranal Observatory and Cerro Tololo Inter-American Observatory in

Chile. The best possible location for ground based observatory on Earth is at Ridge A (a place in the central part of Eastern Antarctica) due to its least atmospheric disturbances and best visibility. Radio observatories Beginning in 1933, radio telescopes were built for use in the field of radio astronomy to observe the Universe in the radio sections of the electromagnetic spectrum, such instruments, or collection of instruments, with supporting facilities such as control centers, visitor housing, data reduction centers, and maintenance facilities are called radio observatories. Radio observatories are also located far from major population centers to avoid EMI from radio waves, TV, radar, and other EMI emitting devices, but unlike optical observatories, radio observatories can be placed in valleys for further EMI shielding. Some of the world's major radio observatories include Jodrell Bank in the UK, the Very Large Array in New Mexico, United States, etc.

2.2.2 Space based solar observatories

Space based solar observatories are telescopes or other instruments that are located in outer space for solar observation, many in orbit around the Earth. Space telescopes can be used to observe astronomical objects at wavelengths of the electromagnetic spectrum that cannot penetrate the Earth's atmosphere and are thus impossible to observe using ground based or airborne based telescopes. The Earth's atmosphere is opaque to a greater portion of UV radiation, X-rays, and gamma rays and is partially opaque to infrared radiation, hence observations of the Sun in these portions of the electromagnetic spectrum are best carried out from a location above the atmosphere of the Earth. Another important aspect of space based solar telescopes is that, because of their location in space, above the Earth's atmosphere, their images are free from the effects of atmospheric effects such as turbulence that plague ground based solar observations. As an outcome, the angular resolution of space based solar telescopes such as the Hubble Space Telescope or the James Web Space Telescope is often much smaller than a ground based solar telescope with a similar aperture. However, space based observatories are much more expensive to build and sustain than ground based solar observatories. Due to their location, space based observatories are also extremely difficult to maintain, e.g Hubble Space Telescope was lucky to be serviced by the Space Shuttles but many other space based telescopes cannot be serviced at all.

2.2.3 Solar Activity

Solar activity is the physical phenomena that occur within the magnetically heated outer atmosphere of the Sun at different time scales. High speed solar wind, sunspots, CMEs and solar flares are some of the basic parameters that govern solar activity. These effects are caused by the magnetic field of the Sun. CMEs and solar flares occur at sunspot groups, coronal holes emit slowly changing high speed streams of solar wind at the surface of the photosphere. High speed streams of solar wind and CMEs both carry the interplanetary magnetic field and plasma outward into the solar system. There are several effects of solar activity on Earth which include the disturbance of radio communications, auroras at and the disruption of electric power. Nonetheless, solar activity have played a major role in the formation and the evolution of our solar system. Solar activity rises and falls within 11 years cycle. An increase in solar activity also increases UV and X-ray emissions from the Sun and this may lead to dramatic effects in our Earth's upper atmosphere such as atmospheric heating which increases the density and temperature of the atmosphere at various spacecraft altitudes and may results to the destruction of satellites in low Earth orbit. Increase in CMEs and the number of solar flares can raise the likelihood that instruments in space may be seriously damaged by accelerated solar energetic particles during the process of solar activity. The SEPs can also affect airline travelers in high altitude, polar routes and the health of astronauts and cosmonauts in space. solar activity also affects terrestrial climate. The change in the total solar irradiance during solar activity maybe too small to cause significant climatic effects but the Earth's climate heats and cools as solar activity rises and falls. The study of solar cycle remains one of the oldest major challenges in astrophysics. The image below shows a summary of the changes in the observations of sunspot from the year 1600 to the year 2000.

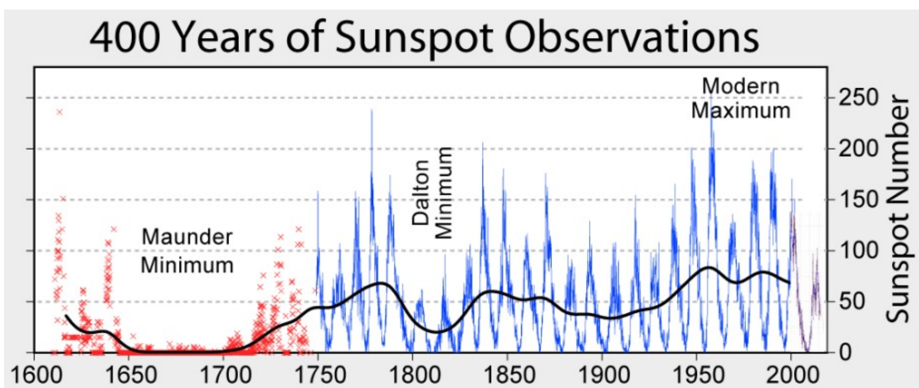

Figure 2.1: 400 years sunspot history, including the Maunder Minimum. This image is from Global Warming Art

.

2.3 Solar Variability

Time series observations of the Sun for many years in several wavelength ranges characterize the Sun as a variable star, beyond doubt (Hudson, 1988). The 11 year variability in the mean number of sunspots visible on the solar disk has been well known for many years (Gilliland, 1982). Back in history, recognition that solar variability may be irregular gained widespread acceptance due to the historical investigations of Eddy (1976) and the confirming evidence due to C-14 measurements (Gilliland, 1982). The recent upsurge of interest in the Sun as a variable star is due to suggestions that not only variations in the magnetic properties occur, but also global changes in the solar radius, effective temperature and luminosity may be occurring (Gilliland, 1982). Variations in the solar constant are also of importance as regards the Earth's climate. The occurrence of changes in global solar parameters due to solar variability may provide useful diagnostics for the theory of stellar structure and stellar evolution. The fact that the solar irradiance at UV wavelengths exhibits significant variations over the solar cycle has been well known for a very long time. In general, changes in the magnetic field flux at the Sun's surface and concentration of the magnetic flux into bright faculae or plages and dark sunspots are understood to be the main drivers of the irradiance variations (Pauluhn and Solanki, 2002), though there are other alternatives. The uniqueness of the UV part of the solar spectrum can not be overemphasized, e.g Sandwiched between the stable radiation and the highly variable energetic short of 1000 A, the EUV and the X-ray, it exhibits a very small but significant variation on different time scales (**?**). Solar UV variability has a significant influence on the atmosphere of the Earth, by being responsible for the dynamics and energetic of the middle atmosphere and it also have an impact on the biosphere (Subbaraya, 1998), Solar UV radiation and its variability is a very important topic of our current day research due to recent developments related to the ozone depletion and global warming phenomena.

2.3.1 Solar UV Irradiance

Solar UV is originating from the sun's corona, upper photosphere, transition zone and chromosphere (Gröbner, 2012). Solar UV emissions have a significant effect on the Earth's thermosphere, stratosphere, mesosphere, and ionosphere. Through excitation, dissociation, and ionization processes, solar UV is the primary source of energy input to the Earth's atmosphere, as a result, it plays an important role in the atmosphere's thermal, vertical and electronic structure. Solar UV irradiance is a principal driver of the strong dynamics in our atmosphere and its cycles of chemical species, like nitrogen and oxygen. UV irradiance varies on 27 day solar rotation and 11 year solar cycle time scales, the wavelength dependent variation is primarily due to the emergence, growth, and the decay of active regions on the solar disk. The Sun also emits the most intense part of UV, Solar EUV. Solar EUV is the solar radiation that covers the wavelengths from 10 nm to about 120 nm of the electromagnetic spectrum. The solar EUV is highly energetic and it is absorbed in the upper atmosphere of Earth, which not only heats the upper atmosphere but also ionizes it, creating the ionosphere. Solar EUV radiation changes by a factor of 10 over the course of solar cycle. This variability produces similar variations in the ionosphere and upper atmosphere. Solar EUV variations are one of the three primary drivers of ionospheric variability. Solar EUV radiation originates in the corona and chromosphere of the atmosphere of the Sun. The Solar EUV spectrum, between 1 nm and 120 nm, is mostly dominated by spectral lines from H, He, O, N, Mg, Si, Fe. The solar EUV photons reach the Earth and are completely absorbed in the upper atmosphere, above 80 km. The thermosphere of the earth, 80km to 600 km in altitude, is heated predominantly by solar EUV radiation. The solar EUV photons also ionizes the atmosphere creating electrons, which form the ionosphere. Solar EUV irradiance varies by as much as an order of magnitude on time scales of minutes to hours (solar flares), days to months (solar rotation), and years to decades (solar cycle). The highly varying solar EUV radiation causes the ionosphere and the thermosphere of the Earth to vary over similar magnitudes and time scales. Because the solar EUV radiation is absorbed by the upper atmosphere, it's impossible to measure from the ground. Thus, its measurements must be made from satellites and rockets. Since it's very difficult to build and maintain sensors that can measure the solar EUV radiation, people relied on proxies for solar EUV such as the Sunspot Number or the F10.7 cm radio flux.

2.3.2 Solar UV Irradiance Variability

Solar irradiance is the dominant energy source on Earth and it's the only external agent of change of its surface and it's atmosphere. The reliable specification of solar irradiance variability on multiple time scales informs a wide range of research and applications Coddington et al. (2019), DeLand et al. (2019), Lean et al. (2020), the most obvious being the attribution of the Sun's natural influence on climate ((Gray et al., 2010);(Matthes et al., 2017)). The observational record of solar irradiance is one of the 22 variables that NASA designates as very crucial for Earth science, and it's an ECV of ESA. Multiple composite records of total solar irradiance since 1978 exist today (Dewitte and Nevens, 2016), (Fröhlich, 2000). There are also records of a few composite solar spectral irradiance reported by DeLand and Cebula (2008) and (Haberreiter et al., 2017) with less fidelity due to the less accuracy of spectral irradiance observations, and since they exist primarily at UV wavelengths, and lack the overlap or the temporal repeatability necessary for direct cross calibration. Many models and proxies have been developed for a better understand and to predict solar UV variations and their wavelength dependence. In spite of the progress, the present estimates of solar UV variability together with atmospheric models still do not provide ideal descriptions of atmospheric phenomena. Hence, we're not sure that the accuracy of the current available measurements are sufficient. Therefore, the need for our nearly ideal measurements. Solar irradiance variations are known to be the main solar factors exerting influence on our Earth's climate, an example is the variability of the UV part of the solar spectrum (Kodera, 2004). According to Krivova et al. (2006), regular monitoring of solar UV irradiance started with the Solar Mesosphere Explorer (Simon et al., 1988), which was operated between 1981 and 1989, but had a low accuracy with an uncertainty in UV irradiance of about 10 percent to 20 percent. With the launch of UARS in 1991 more reliable data became available. Daily measurements at around 120 nm 400 nm were then carried out by two instruments, SUSIM (Brueckner et al., 1993) and SOLSTICE (Simon et al., 1988). They both provided important information on the absolute level of the solar UV irradiance and the degree of its variation with time. The Sun's total (integrated over all wavelengths) irradiance changes by about 0.1 percent over the course of the solar cycle ((Shukure et al., 2021b):(Marchenko et al., 2022)), The Sun's UV irradiance varies by a few percent within 200 nm to 300 nm, 10 percent to 20 percent at 150 nm to 200 nm and more than 50 percent around the near 121.6 nm (Floyd et al., 2004). The amplitude of variations at 300 nm to 400 nm remains unclear since it is below the uncertainty of both instruments, which is about 2 to 3 percent (Canter and Wood, 1996). These solar UV irradiance records remain too short to allow conclusions about the influence of irradiance variations on our climate. Hence the need for the help of models. Some of the most models of TSI, which have made great strides toward understanding and reproducing observed irradiance variations on time scales of days to decades are Shukure et al. (2021b):Marchenko et al. (2022), Solanki et al. (2004), Usoskin et al. (2005). Some models up to the Maunder minimum have also been developed that reconstruct the cyclic component of the irradiance variations on longer time scales (Lockwood and Stamper, 1999), (Solanki and Fligge, 1999), (Solanki et al., 2000), (Lean, 2000) . Two problems with the modeling of solar UV irradiance are: 1) between 300 nm and 400 nm SUSIM data display a far smaller variability than the models (due to insufficient sensitivity of the measurements); 2) models at shorter wavelengths are rather simple but less successful. On long time scales, estimates of solar UV irradiance are usually scaled from total irradiance reconstructions or based on linear or multiple regressions with proxy records (Lean, 2000). On shorter time scales, models are generally more complex. Often, Ca II K filter grams are used to extract information on the evolution of active regions and later converted into irradiance (Worden et al., 1998). These models turn to reproduce observations very well, which indicates that the main driver of the solar UV irradiance variations is the surface magnetic activity.

2.4 Possible causes of Solar UV Irradiance Variability

The Sun is the strongest or the main source of UV radiation in our environment. Emissions from the Sun include heat, visible light and UV radiation. Visible light is made up of different colours as seen in the rainbow while the ultraviolet radiation spectrum is divided into three sections namely UVA (315-400nm), UVB (280-315nm) and UVC (100-280nm). As the Sun's rays pass through the Earth's atmosphere, all UVC and most of the UVB are absorbed by the ozone layer of the Earth, oxygen, water vapour and carbon dioxide. UVA is the not filtered by the Earth's atmosphere, thereby accounting for about 95 percent of the UV radiation reaching the Earth's surface. It is well understood that sunspots and faculae are the primary sources of solar irradiance variability and that model parameterizations of these magnetic features readily reproduce the observations. As the fidelity of a model's sunspot and faculae representations improves, its ability also improves to reproduce observed irradiance variability (Coddington et al., 2019). In more details, the primary sources of solar irradiance variability are bright faculae in compact plage and an extended network, and the central umbra and the surrounding penumbra of dark sunspots. Solar irradiance varies since the solar activity alters the occurrence of the above magnetic features and hence their local emission relative to the Sun's quiet background emission. As these features erupt, evolve, and rotate on the solar hemisphere during the progression of the activity cycle of the Sun, the projection at Earth of the altered local radiative output in the faculae and the sunspots respectively increases and decreases the solar irradiance. A variety of evidence in historical proxies of solar activity suggests that the quiet Sun irradiance may not be invariant on multi decadal time scales (Lean et al., 2005).

2.5 Solar Activity Models

Reviewing the dynamo models for solar cycle modulations beyond 11 year periodicity which are long-term variations of the solar cycle include: grand minima, grand maxima, the Gnevyshev–Ohl/Even–Odd rule, Suess cycles, and Gleissberg cycle Karak (2023). The most important and fundamental feature of the solar magnetic field is its 11 year cyclic oscillation. Observations of large-scale solar magnetic field since the 1950s, showed the reversals of the magnetic field. But the times of the revealed reversals and the strength of the magnetic field are not the same for all the cycles. The group sunspot number since 1610 and the area since 1874 also reveals cycle-to-cycle variations (Hathaway, 2015) as seen in the figure below.

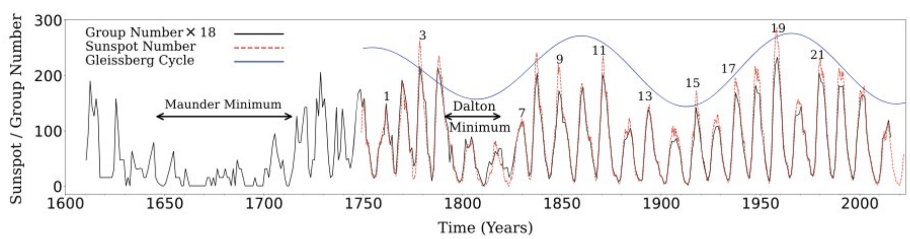

Figure 2.2: Yearly variation of the monthly mean sunspot number smoothed using a Gaussian filter of FWHM = 7 months (red curve), available since 1749 and the yearly mean group sunspot number (black curve) available during 1610–2015. Note that group number is scaled by a factor of 18 to bring it to the scale of sunspot number. The blue curve with 98-year period guides the Gleissberg cycle. Cycle numbers for which the Even–Odd effect is obeyed are shown by tagging the number on the odd cycles. Source: (Karak, 2023)

Hence, the 11 year solar cycle is not regular which makes the prediction of the future solar cycle a formidable task (Petrovay, 2020). The prediction of solar cycle is very essential since the magnetic field of the Sun drives the space weather which causes very serious problems to us humans, by damaging our satellite's electronics, GPS networks, telecommunications, and electric power grids at high latitudes, making polar routes significantly dangerous for aviation, increasing the radiation dose to astronauts in space etc (Temmer, 2021). Evidence also suggests that the variable solar activity may drive changes in our Earth's global temperature (Solanki et al., 2013). Some of the main distinct features of solar cycle which can be considered as extreme examples of irregularity are grand minima and grand maxima.

Additionally, there are also some long-term patterns beyond the 11 year variation, such as Suess cycles, Gnevyshev–Ohl rule and Gleissberg cycle which the readers can check the excellent reviews (Biswas et al., 2023) for further discussion. Grand minima are extended episodes of significantly lower magnetic activity than the normal one, the best example is the Maunder minimum in the 17th century which occurred when solar activity was very weak than the normal one for about 70 years (Eddy, 1976). Several observations have also shown that the Maunder minimum was not complete due to lack of activity since the Sun was still producing spots and cycles at a lower rate (Zolotova and Ponyavin, 2016). The Maunder minimum (and probably all grand minima) is a distinct and a special state of solar activity (Karak, 2023) because: (1) There was a very strong hemispheric asymmetry during the latter half of the Maunder minimum; and sunspots were observed mostly in the southern hemisphere (Ribes and Nesme-Ribes, 1993). (2) The recovery of the Maunder minimum is gradual, though the onset is uncertain. Some previous results suggested that the onset is abrupt (Usoskin et al., 2004), while other later studies showed that the onset is likely to be gradual (Vaquero et al., 2011). (3) A proxy of solar activity inferred from a cosmogenic isotope C-14 showed that the cycle length before the onset of Maunder minimum was longer than its usual value (Krivova et al., 2021). Analyses of C-14 for the last 11,400 years also revealed the following important results (Usoskin et al., 2007): (1) The Sun spent about 17 percent of its time in the grand minimum state. (2) Grand minima are of two types: short minima of Maunder type with a duration of 30–90 years and long (>100 years) minima of Spörer type. (3) The grand minima recur aperiodically. (4) The waiting time distribution of the occurrence of grand minima displays a significant deviation from an exponential distribution. (Moss et al., 2008) also showed that feature (5) may be an artifact of poor statistics (it is based on only 27 grand minima identified in the observed data). On the other hand, grand maxima are extended periods with higher magnetic activity than the normal one. The modern maximum which occurred around 1960 is an example of this. In about 11,000 years ago, 23 grand maxima were detected and the Sun spent appreciably 12 percent of its time in this phase (Usoskin et al., 2023). Grand minima are more long-lived than the grand maxima (Solanki et al., 2004). The distribution of the duration of grand maxima shows a very smooth variation with an exponential fall at longer durations while the distribution of the waiting time between the consecutive grand maxima is not conclusive but there is an indication of deviation from the exponential law. Indicators of solar activity (Hathaway and Rightmire, 2010) also shows the 11 year activity cycle of the Sun which is a manifestation of the solar dynamo. This includes, the sunspot area and the number, coronal and chromospheric indices such as the Mg II index, F10.7 cm radio flux, X- ray flux, and solar irradiance. Soar surface magnetic flux evolution plays a dominant role in the variability of solar UV irradiance (Marchenko et al., 2022).

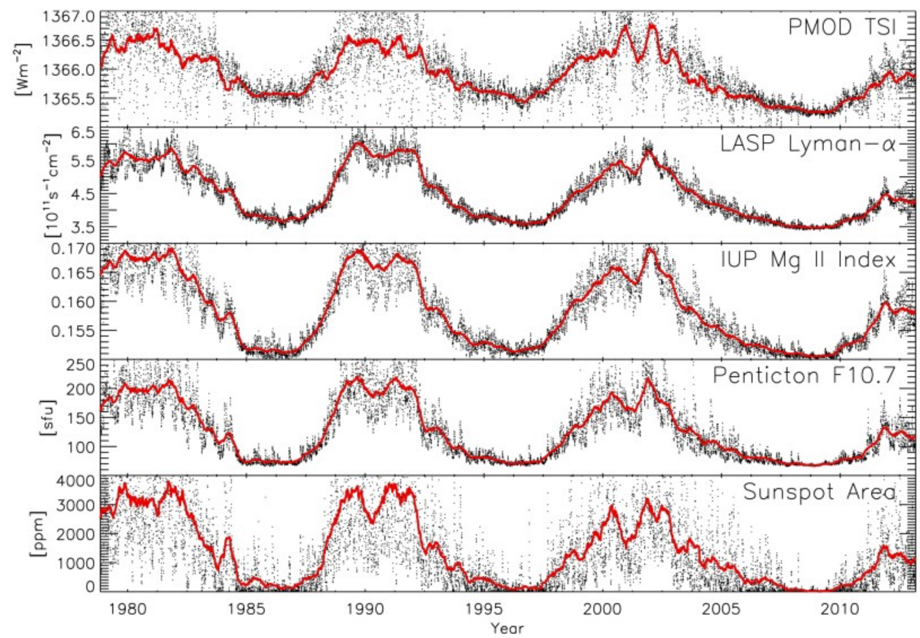

Figure 2.3: Indices of solar activity. From top to bottom, the composite (version $d41_6 2_1 302$, Fröhlich (2000), the LASP Lyman-α irradiance composite Gordon et al. (2000), the IUP Mg II index composite (version 4, Viereck and Puga (1999), Skupin et al. (2005)), the Ottawa and Penticton adjusted 10.7 cm radio flux record (Tapping (1987), Tapping (2013)) and the projected sunspot area composite by Muñoz-Jaramillo et al. (2013) (version 0613). The red curves follow the 181-day moving mean.

2.5.1 Magnesium II core-to-wing ratio

MgII index plays an important role as a proxy for solar activity. It correlates well with the EUV which is crucial for understanding the upper atmosphere.

EUV is the primary energy input to the Earth's upper atmosphere. Variations in the Sun's EUV flux drive the chemistry and the dynamics of the Earth thermosphere and ionosphere. Ionization of the neutral atmosphere by the EUV flux on the daylight side of the Earth contributes to the creation of the ionosphere. According to (Lean et al., 2011), over the eleven year solar cycle, the EUV irradiance changes by a factor of 2–5 depending on wavelength.

Atmospheric modelers have had to rely on a more commonly available measurement which can be used to represent the true EUV irradiance. (Heath and Schlesinger, 1986) identified the Magnesium II core-to-wing ratio as a useful proxy for the solar EUV irradiance. This ratio is also known as the MgII index.

Despite the importance of MgII index as a proxy for solar activity on EUV, studies find that there are still some discrepancies with MgII (Snow et al., 2014).

2.5.2 F10.7

F10.7 refers to the F10.7 cm radio flux which is a measure of solar radio emissions at a wavelength of 10.7 cm. It is a proxy for overall solar activity, including sunspots and solar flares. F10.7 is among the most widely used indices or proxies of solar activity. Its applications also include use as a simple activity level indicator and as a proxy for other solar emissions. Or quantities which are more difficult to obtain, and also as a commonly available datum for antenna calibration (Tapping, 1987). Comparing F10.7 with other solar proxies by Brueckner et al. (1993) analysis, they found a cyclic drop to its minimum value.

2.5.3 CaII K lines

Solar Ca II K line is a broad absorption line located at the short-wavelength end of the optical range (Kakuwa and Ueno, 2022). Ca K line is one of the proxies of solar magnetic activity. It's bright in active regions, including plages and enhanced network regions, and also in quiet-Sun network lanes in our chromosphere. Continuous UV observations by satellites began around 1980 (DeLand et al., 2020). Long-term UV irradiance is significant in the context of Sun to Earth or star to planet relations (Lilensten et al., 2007). Solar UV radiation shows comparatively large quantitative and fractional variations with solar cycles than other wavelengths (Fröhlich and Lean, 2004).

Based on several studies including a comparative study of two solar activity with proxies by Pietrow et al. (2024), indications of an upward bias in the solar activity statistics was found. And this was based on the activity indices derived from the CaII H and K lines.

A study of the influence of solar surface magnetic flux (SFD) on TSI was done by Shukure et al. (2021a). They characterized the influence of the magnetic flux density variation on the TSI using the Pearson, Spearman, and percentage bend correlations and wavelet analysis between the TSI and the flux density. This did not include the influence of solar surface magnetic flux density on solar surface UV variability.

In order to cover these discrepancies, we introduce a new model; solar magnetic flux density.

2.5.4 Solar Surface Magnetic Flux Density

This refers to the strength of the magnetic fields on the solar surface. It's units of measurements are either Gauss per Pixel. Magnetic fields on the surface of the Sun are generated by the movement of charged particles within Sun's interior, primarily through processes related to differential rotation and convection.

As discussed in chapter one, Solar UV irradiance is the amount of ultraviolet radiation emitted by the Sun and reaching our Earth's atmosphere. It's measured in Watts per meter square.

This study signifies as a backbone in advancing the knowledge of the scientific community to understand the interaction between the strength of surface magnetic field and UV variability in sun-like stars throughout the universe.
It's a breakthrough for the preservation of life both on earth and in space as it will help us to prepare more in advanced and take more precautionary measures every period before high solar activity.
This research is also important for scientists to know the period to observe and study stars in the UV spectrum.
This research gives us a significant lift in the way that we understand our planet, especially during phenomena like solar storms.

This thesis fall-short of the study of solar interior (core, radiative zone and convective zone), thereby focusing on regions of weak and strong magnetic magnetic fields on the solar surface. It covers the influence of magnetic features (such as solar activity) from the photosphere of the sun to its corona and possibly its effects on our planet. This project focuses mainly on the UV spectrum of the sun and its variability, as influenced by solar surface magnetic flux density..

Delving into the intricate relationship between solar surface magnetic flux density and solar UV variability, let's discuss an overview of solar magnetic activity and solar ultraviolet (UV) radiation emitted by the Sun. Here are the following key points to note:

Chapter 3

Methodology

3.1 Data and Instruments

3.1.1 The Magnetic Flux Density

Since Hale (1908) discovered magnetism in sunspots, it's been well understood that magnetic flux can be detected everywhere in the Sun's photosphere, as explained by Stenflo (2017).

At the moment, optical instruments are the primary tools used to measure magnetic flux in the photosphere of the Sun (Shukure et al., 2021a). The data of the magnetic flux used in this project was collected from the HMI/SDO instrument with a spatial resolution of 1:·

All data used for this project corresponds to the years 2010 and 2014, during solar minimum and solar maximum respectively, for SC 24. The magnetism data was designed and calibrated by Schou et al. (2012). In 2010, SDO/HMI started providing data in the fifth month of the year, this is the reason why the analyzed data of the year 2010 started from the May 01. Following the magnetic flux threshold defined by Kutsenko and Abramenko (2016) and following the method used by others such as Howard et al. (1985).

3.1.2 Solar Surface UV Irradiance

As documented by Snow et al. (2022), the daily Solar UV irradiance data for 2010 and 2014 data used in this project is from SOLSTICE, one of four solar irradiance measurement experiments launched as part of SORCE on January 25, 2003. SORCE SOLSTICE was a follow-on to the successful SOLSTICE launched aboard the UARS in 1991 (Rottman et al., 1993). The new SOLSTICE made daily solar UV (115-320 nm) irradiance measurements and compared them to the irradiance from an ensemble of other 18 stable early-type stars in the universe. This unique approach provided an accurate monitor of instrument in-flight performance and also provided a basis for solar-stellar irradiance comparison for future generations. The data is shared by SORCE

SOLSTICE FUV Level 3 Solar Spectral Irradiance Daily Means V018, Greenbelt, MD, USA, GES DISC. It's important to note that the SSI data used in this project covers both the FUV and MUV ranges (115-320 nm), that is (FUV: 115 – 180 nm and MUV: 180 – 320 nm) for both years, since this wavelengths give a more important understanding and precise knowledge for processes on the solar atmosphere (Thiemann et al., 2023).

3.1.3 Solar Activity Indices Used in this Thesis

One of the proxies used in this project is the F10.7, constructed from total sunspot area by Yeo et al. (2020). The solar radio flux at 10.7 cm (2800 MHz), often called the F10.7 index, is one of the proxies often used as an indicator of solar activity. Other similar proxies for solar chromospheric variability used are MgII index and CaII K lines.

3.2 Methods of Data Analysis

3.2.1 Cross Correlation analysis

Correlogram is a chart of correlation statistics suitably used for checking the randomness in a dataset. If the dataset is random, then auto-correlations will be near zero for any and all time-lag separations. If the dataset is non-random, then one or more of the auto-correlations will be significantly non-zero. The correlogram analysis method can help us answer the following questions:

Are the datasets random?

Is there an observation related to an adjacent observation?

Is the observed time series sinusoidal?

Is the observed time series auto-regressive?

Also called Pearson's Correlation, the known Pearson's correlation between signals has been used. This method is used to determine the mutual correlation between two signals according to Peterson et al. (1998). This method is more important since there is no need to worry about data gaps. With this method, Pearson's and Spearman's correlations for each pair of variables with are computed. Pearson's correlation measures the linear correlation between two variables, while Spearman's correlation measures the monotonic relationship between the two variables (Shukure et al., 2021a). The toolbox also computes percentile bootstrap 95% confidence level for each correlation. The CI gives an alternative way to test the null hypothesis. The pairs of observations are then resampled with replacement and their correlation values obtained.

3.2.2 Continuous wavelet transform (CWT)

This tool provides an over-complete representation of a signal by letting the translation and scale parameter of the wavelets vary continuously. It has zero mean localized in both frequency and time. The uncertainty principle indicates that there is always a balance between localization in time and frequency (Addison, 2017); (Merry, 2005). The CWT is a very powerful tool for non-stationary signals and gives information about the behavior of intermittency and periodic phenomena present in two signals (Torrence and Compo, 1998).

$$Wx(s,b) = 1/s \int x(t) Q^* [(t-b)/s] \, dt \tag{3.1}$$

where x(t) is the time–frequency domain, s and b are the scale and time, respectively, and Q* is the complex conjugate of the mother wavelet Q.

3.2.3 Cross Wavelet Transfor (XWT)

The XWT is proposed as a data analysis technique, an analysis method used to compare signals and to find regions where the time series show high common power. The XWT was applied in order to indicate the common power and the relative phase between signals in time–frequency space. The XWT between two time series x(t) and y(t) therefore given by:

$$W^{xy} = W^x W^{y*} \tag{3.2}$$

where * denotes the complex conjugate. The cross-wavelet power is defined as W^{xy}. The complex argument $\arg(W^{xy})$ is interpreted as the local relative phase between x(t) and y(t) in the time–frequency domain (Grinsted et al., 2004). A python code was developed for the wavelet analysis.

3.3 Pearson and Spearman correlation coefficient

The Spearman correlation coefficient assesses the monotonic relationship between the signals. It is less sensitive to outliers compared to Pearson correlation. Similar to Pearson, Spearman P-value tests the significance of the Spearman correlation.

The Spearman correlation indicates whether the relationship between the two signals in each plots is monotonic (consistently increasing or decreasing) even if not perfectly linear, The p-values for both correlations in each plots help determine if the observed relationships are statistically significant, reducing the likelihood that they maybe due to random chances.

The Pearson correlation coefficients quantifies the strength and direction of the linear relationships between the two signals in each diagram for figure 4.2, and figure 4.3 for both 2010 and 2014. While the Pearson P-values Indicate the statistical significance of the correlation in each figure. A small p-value (typically < 0.05) suggests that the correlation is statistically significant, while a P-vale > 0.05 suggests that the correlation is less significant (Shukure et al., 2021a). All the are recorded in Tables 4.1 and 4.2.

In this project, specific invalid values (-99.00000) are replaced with NaNs, representing the days of non available data for the signal. Linear interpolation is then used to handle NaN values ensuring a continuous dataset for 2010. The data is normalized to have a mean of 0 and a standard deviation of 1, resulting in the signal. The cross-correlation between the signals is calculated using the correlate function from NumPy.

Chapter 4

Results and Discussions

4.1 Characterizing the Influence of Solar Surface Magnetic Flux Density on Solar UV Irradiance variability

In this section, we present the detail of the results and discuss our findings. Mainly we focuss on the trend analysis, wavelet, and correlogram analysis.

4.1.1 Trend Analysis

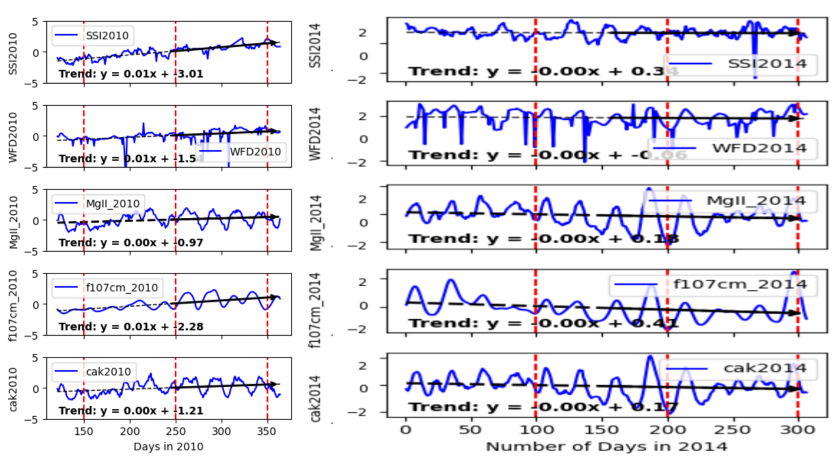

Figure 4.1: Trends Relationship for SSI, WFD and Solar UV Proxies in 2010 (LHS) and 2014 (RHS)

Figure 4.1 shows a gradual increase over the year, from May 1st to December 31, 2010, indicating a rise in solar activity (Ansor et al., 2023). Within the same period, the trend of SSI shows a sharp increase, suggesting increased emissions of solar surface UV radiations.

In the same manner, the trend of Magnesium II Index shows a slight increase, indicating a rise in chromospheric activity over the year in 2010. Mg II index measures the emission in the core of the magnesium II line, which is a good proxy for solar chromospheric activity (Snow et al., 2014).

The trend line of F10.7 shows a slight upward trend, indicating an increase in solar activity over the year in 2010.

The trend of Calcium II K shows a slight upward trend, similar to the Mg II index, indicating an increase in chromospheric activity over the year in 2010 due to an increase in the intensity of the Ca II K line.

The consistent upward trends in the SSI, MgII, f10.7, and Ca II K line in 2010 indicate a general increase in solar activity during 2010. This increase is likely associated with the solar surface magnetic field. The year 2010 corresponds to the rising phase of Solar Cycle 24, leading up to its maximum around 2014.

The correlations between the different signals (SSI, MgII, f10.7 and CaK) suggest that the various measures of solar activity are interconnected. For instance, increased chromospheric activity (MgII and Ca II K lines) typically accompanies higher levels of SSI and greater solar radio emissions (F10.7).

Therefore, the analysis of these signals from 2010 reveals an overall increase in solar activity influenced by WFD, characteristic of the solar minima of solar cycle 24. The different proxies for solar activity, including spectral irradiance, chromospheric indices, and radio flux, all point towards a cohesive rise in solar activity. Understanding these relationships helps solar physicists predict space weather and its potential impacts on Earth's environment and technology.

In the same way, the RHS of figure 4.1 represents the trends relationship for the SSI, WFD, MgII and CaII K lines in 2014 with all decreasing trends, having the reverse explanations with the year 2010.

4.1.2 Correlation Analysis

The main focuss of this sub topic is to present the cross correlation between the intended parameters. In the title, the correlation coefficient and some statistical value are addressed.

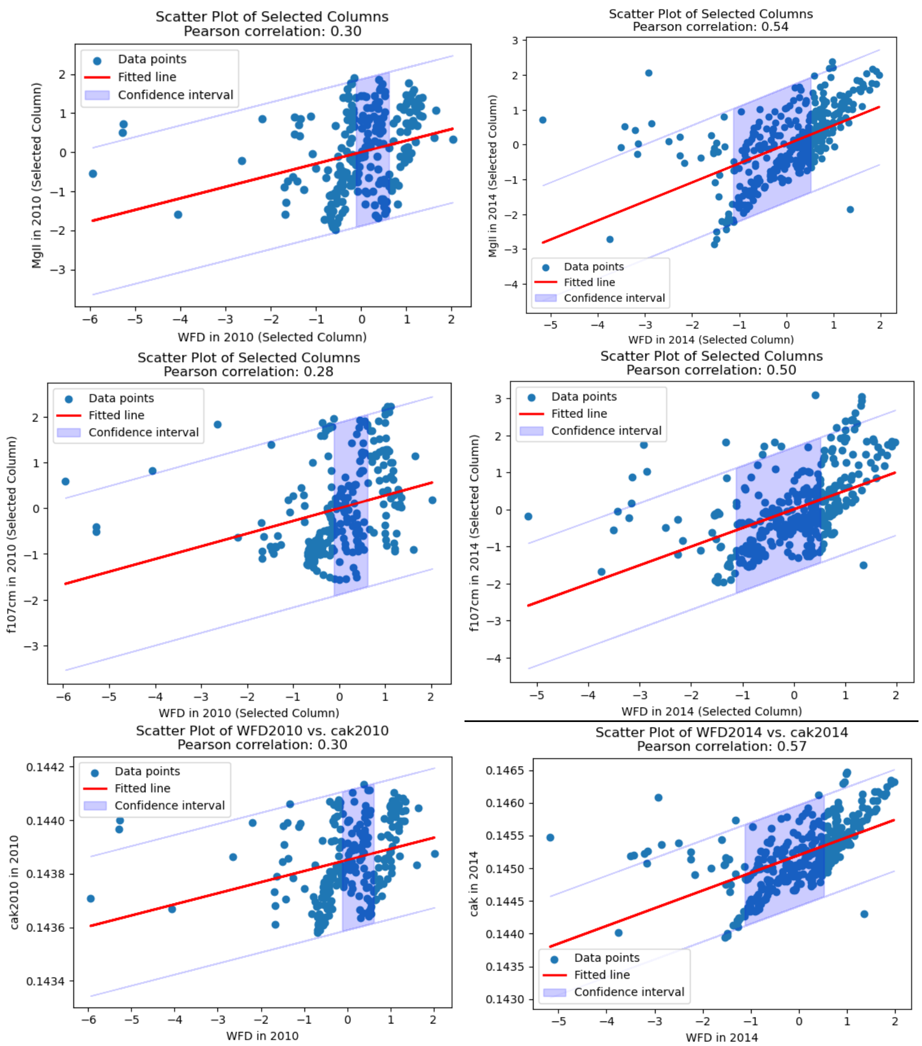

Figure 4.2: Scatter Plots for WFD and Solar UV Proxies in 2010 (LHS) and 2014 (RHS)

Figures 4.2 and 4.3 provide the relationships between the signals, focusing on specific columns from each dataset. The white lines represent the COI, and the region above the COI is more significant. The analysis involves several steps, including interpolation, correlation calculation, linear regression, and plotting.

The red lines in the plots represents the best-fit linear model, while the shaded blue regions around the fitted line in the plots represents the range within which the true regression line lies with 95% confidence. The Pearson correlation coefficients and the fitted line in the scatter plots reveal the degree to which each of the signals are related.

The linear regression model and confidence intervals for each plots provide predictive insights, showing how the signals are related. MgII, f10.7, CaII K lines are solar activity indicators.

By studying the relationships between signals on each plot, solar astrophysicists can better understand the dynamics of solar variability and its impacts on the solar-terrestrial environment. In Figure 4.2, the red lines represent increasing trends, these trend lines provide insights that all the signals are relatively increasing over the years 2010 and 2014, indicate notable linear events where significant changes are occurring. The strength of this relationships is indicated by Pearson P-value, Spearman P-value, Spearman correlation coefficient, all are indicated in Table 4.1. The indicated Pearson correlation coefficient on each graph is more sensitive in indicating the relationships between each signal. Pearson correlation coefficients of WFD-MgII, WFD- CaK are 0.30 each in 2010, indicating a stable relationship between the signals, while that of WFD-f10.7 which gives 0.28 is the lowest and it indicates a weak relationship between the signals. While in 2014, all the signals have Spearson correlation coefficient of 0.54 for WFD-MgII, 0.50 for WFD-f10.7 and the highest of 0.57 for WFD-CaK, indicating a significant relationship between the signals, with increasing solar activities.

Figure 4.3 shows the correlation analysis between solar indices and UV irradiance.. Strong correlations between them, with Pearson correlation coefficient from 0.46, imply coherent changes in the solar atmosphere, from the photosphere (SSI) to the chromosphere (Mg II and Ca K indices) and the corona (F10.7 cm radio flux). The trends indicate whether solar activity was increasing or decreasing over 2010 and 2014. For example, increasing trends in the SSI-WFD suggest rising solar activity, this is also reflected in the trends of other signals. Consistent trends and correlations across these signals reinforce the understanding that solar activity affects various layers of the solar atmosphere and can be tracked using multiple observational proxies.

WFD measures aspects of solar emissions. A correlation between WFD and SSI indicate that weak flux densities are influencing the emissions of solar UV irradiance. Mg II Index is indicates and increase in solar UV irradiance. Strong correlations between MgII and SSI suggest that MUV irradiance changes track with chromospheric activity as measured by the Mg II index. F10.7 cm Radio Flux is a proxies for solar activity, with the radio flux often used to infer changes in solar output that affect space weather and ionospheric conditions, a positive correlation between F10.9 with SSI indicates that F10.9 influences SSI positively.

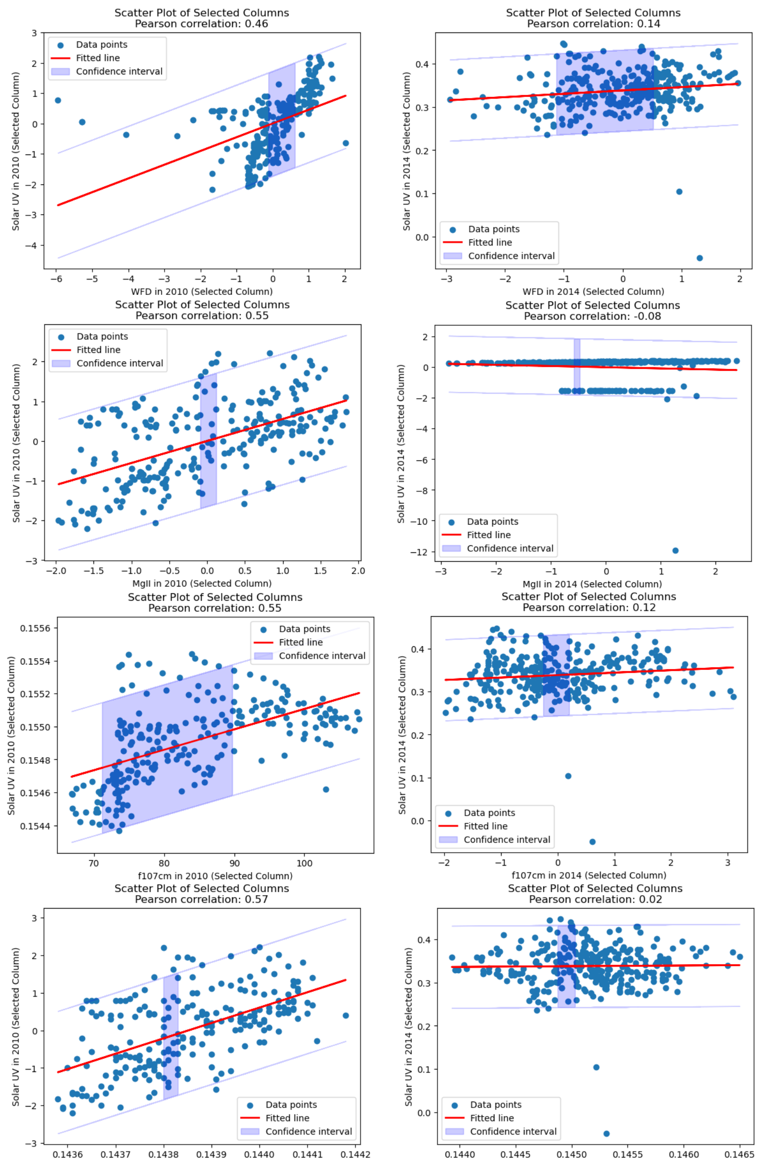

Figure 4.3: Scatter Plots for SSI, WFD and Solar UV Proxies in 2010 (LHS) and 2014 (RHS)

Ca K Index reflects chromospheric activity with potential correlations indicating consistent solar behavior of SSI across different emission lines.

Similar trends for SSI-WFD, SSI-MgII and SSI-f10.7 could mean they respond similarly to solar activity changes in 2010 and 2014 and same with SSI-CaK in 2010. While the negative trend of SS-CaK in 2014 indicates a lag in response, indicating how slowly it reacts to changes in solar activity compared to the rest of the signals.

4.1.3 Continuous Wavelet Transform

Figures 4.4 and 4.5 show the CWT performed on our normalized signals in both 2010 and 2014, and they also indicate the magnitudes of the coefficients of the signals. The visible regions above the squared black lines in all subplots b) and d) in Figures 4.4 and 4.5 are the 95% COI. The color intensity represents the magnitude of the wavelet coefficients, with brighter colors (yellow) indicating higher magnitudes. This highlights stronger oscillatory components at those periods and times. The y-axes show different periods that reveal the dominant periodicities in the data. For example, bright regions around periods of 25-35 days clearly seen in all signals, indicate a strong periodic oscillation of the Sun (Guharay et al., 2020) or solar rotation in 2010 and 2014. While the x-axes allow observation of how these oscillations vary over time, in days. Strong vertical streaks indicate sustained oscillations at specific periods.

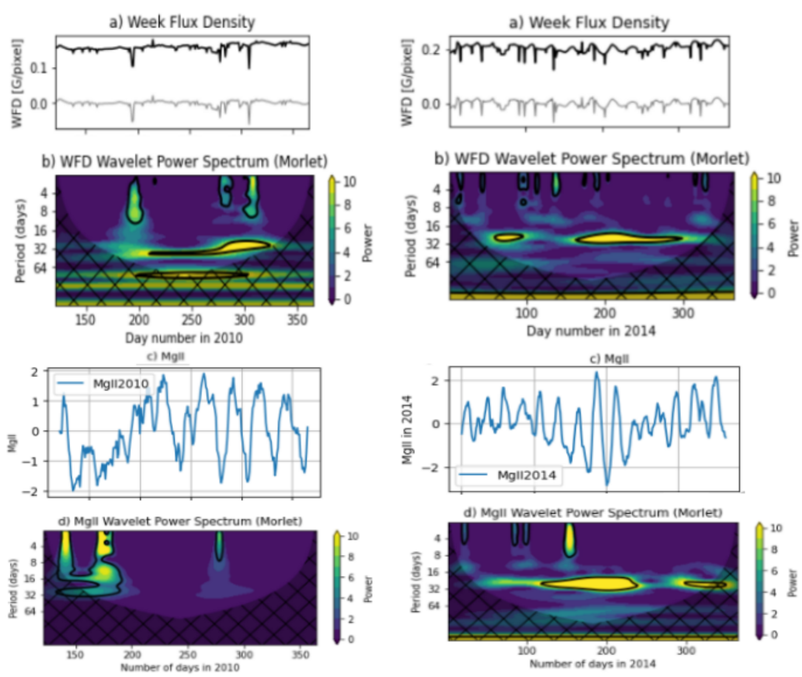

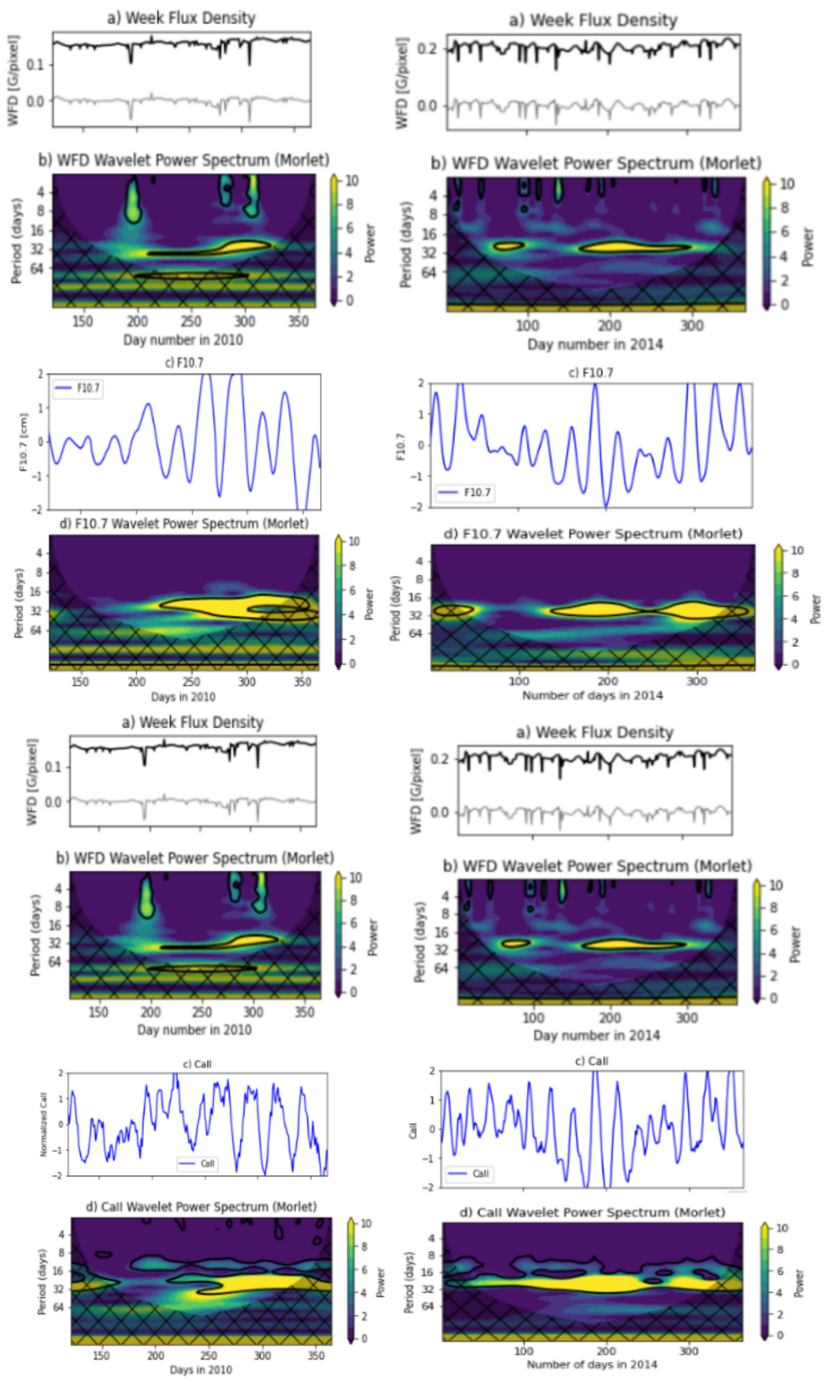

Figure 4.4: CWT for WFD and Solar UV Proxies in 2010 (LHS) and 2014 (RHS)

By comparing each pair of the plots (subplots b) and d)) in both years, we can examine common periods where both signals have high magnitudes, indicating synchronized oscillatory behavior between them. If the bright regions in both figures align well in both period and time, this suggests that the signals not only oscillate with similar periods but also have a strong relationship, variations in the patterns over time, indicating how the relationship between the signals changes throughout the year. For example, certain periods being prominent only in specific months can hint at seasonal or periodic influences affecting both signals.

For each signal pares in both figure 4.4 and figure 4.5, there are significant power regions at periods around 4-64 days and high or stronger power regions are evident around days 25 to days 35. The stronger periods indicate that the peaks and troughs in both signals occur simultaneously, reflecting a synchronized or coupled behavior between each of the two signals in comparison. Both plots show a similar range with consistent magnitude, indicating the comparability and intensity of fluctuations in all signals.

Let us consider the signal pares of Solar UV irradiance and WFD in 2010 and 2014 (subplots b) and d) in page 53), in which the study of other signals can be reflected. We see that the synchronization of periods and the concurrent high power regions of these signals suggest that the Solar UV irradiance and WFD signals are likely influenced by the same solar activity cycles or phenomena. This could include solar rotation (for dominant similarities within periodicities of 27 days), active regions, or other solar magnetic activity.

The observed periodicities out of the range within 25 to 35 days might be linked to quasi-periodic variations observed in solar activity, such as the Rieger-type periodicities Gurgenashvili et al. (2021) or rotational modulation of solar emissions, and even due to noise and data issues. Since WFD is a measure of weak flux densities in solar emissions, its strong correlation and synchronization with Solar UV irradiance imply that WFD can be a reliable proxy for studying solar UV variations and overall solar activity.

Finally, the CWT analysis of Solar UV and WFD reveals a strong relationship between these signals, characterized by synchronized periodicities and concurrent high power regions. This indicates that both signals are likely governed by similar solar activity cycles, providing valuable insights into the dynamics of solar emissions and their underlying mechanisms. The similarity in their CWT profiles underscores the interconnected nature of different solar emissions and the utility of WFD as a proxy for solar UV studies.

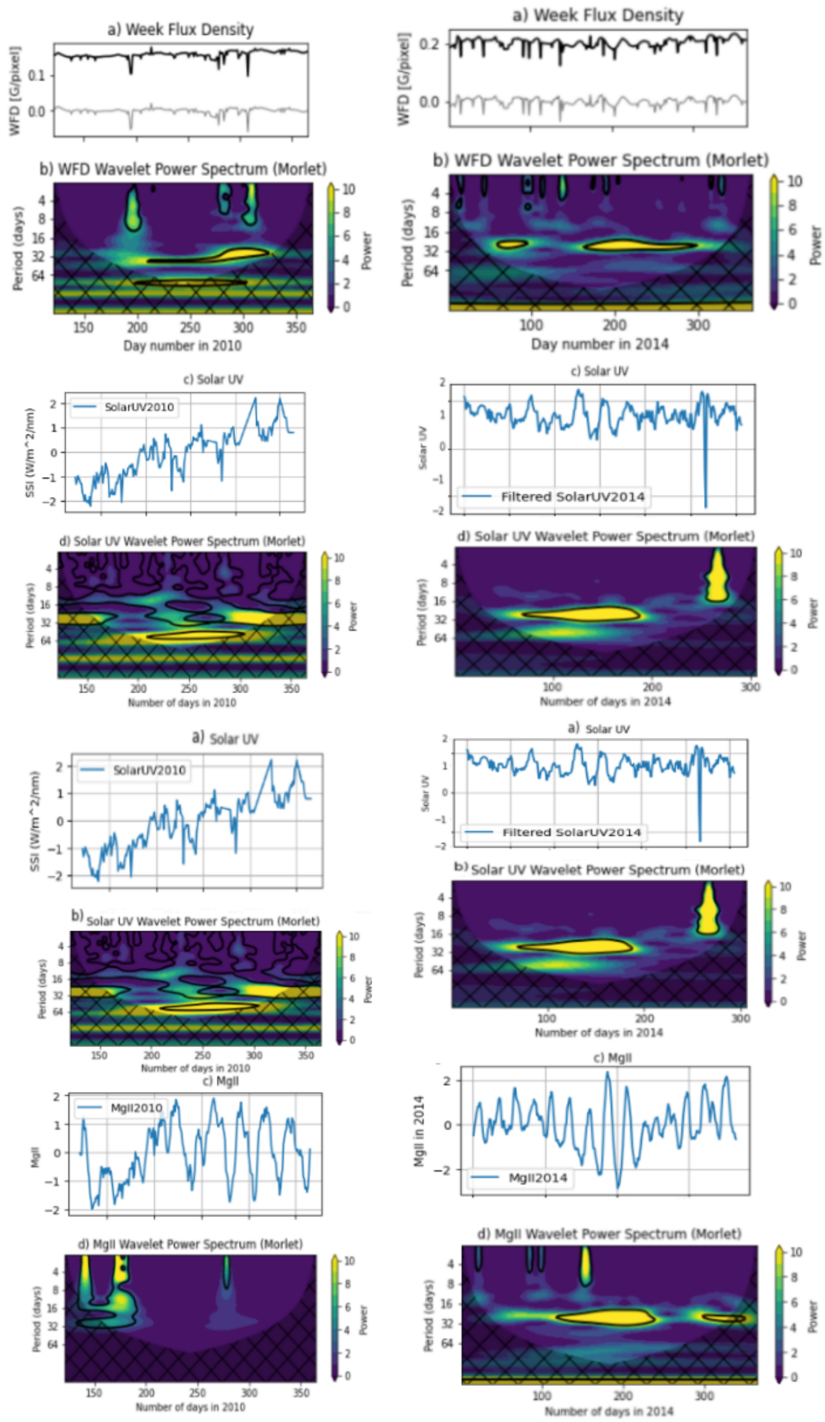

a) Week Flux Density
WFD [G/pixel]
b) WFD Wavelet Power Spectrum (Morlet)
Period (days)
Power
Day number in 2010
c) Solar UV
SolarUV2010
SSI (W/m^2/nm)
d) Solar UV Wavelet Power Spectrum (Morlet)
Number of days in 2010
a) Solar UV
b) Solar UV Wavelet Power Spectrum (Morlet)
c) MgII
MgII2010
MgII
d) MgII Wavelet Power Spectrum (Morlet)
a) Week Flux Density
b) WFD Wavelet Power Spectrum (Morlet)
Day number in 2014
c) Solar UV
Solar UV
Filtered SolarUV2014
d) Solar UV Wavelet Power Spectrum (Morlet)
Number of days in 2014
a) Solar UV
b) Solar UV Wavelet Power Spectrum (Morlet)
c) MgII
MgII in 2014
MgII2014
d) MgII Wavelet Power Spectrum (Morlet)

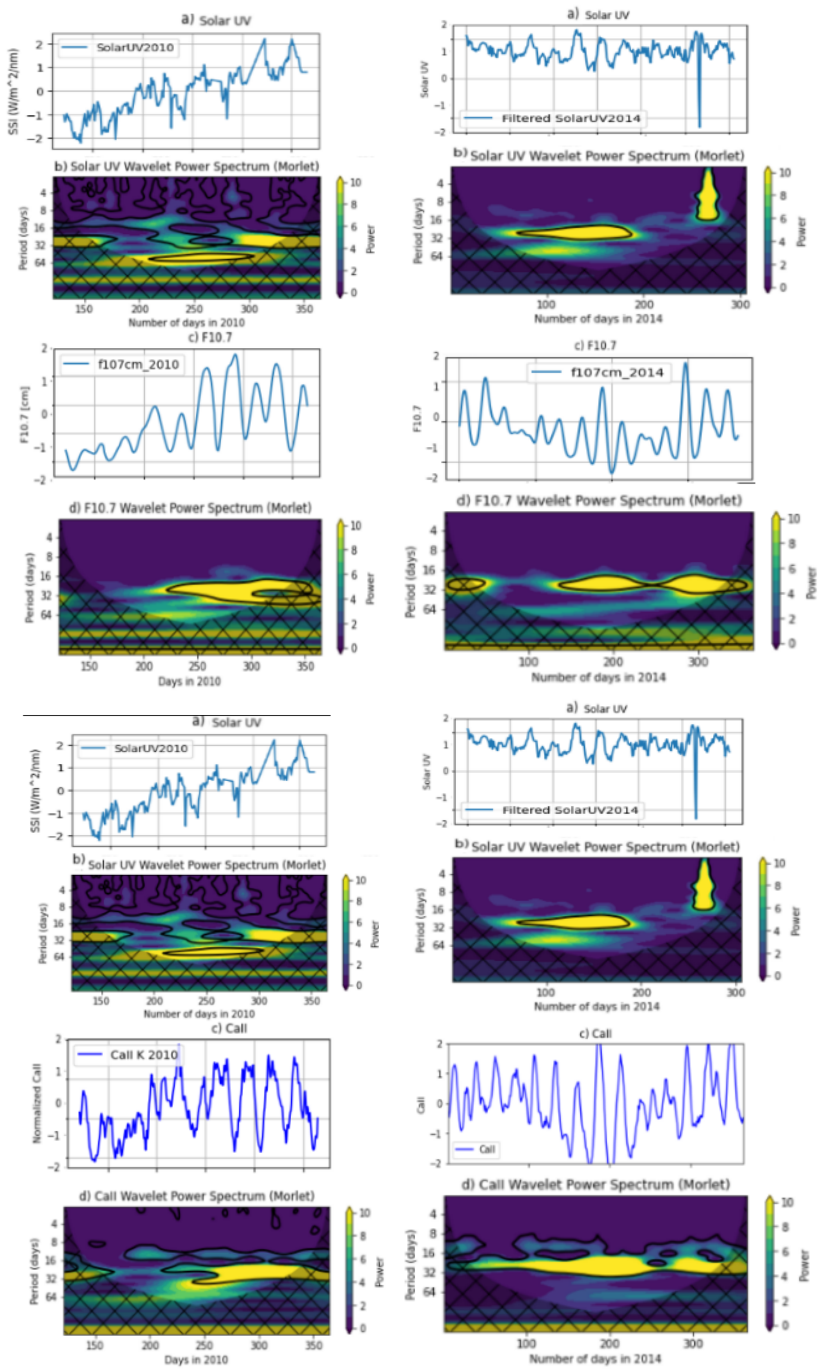

Figure 4.5: CWT for SSI and SSI Proxies in 2010 (LHS) and 2014 (RHS)

4.2 The Casualty Linkage Between Solar Surface Magnetic Flux and Solar UV Irradiance Variability

In this section, we shed light on the specific characteristics emerging from the interaction between two sets of data.

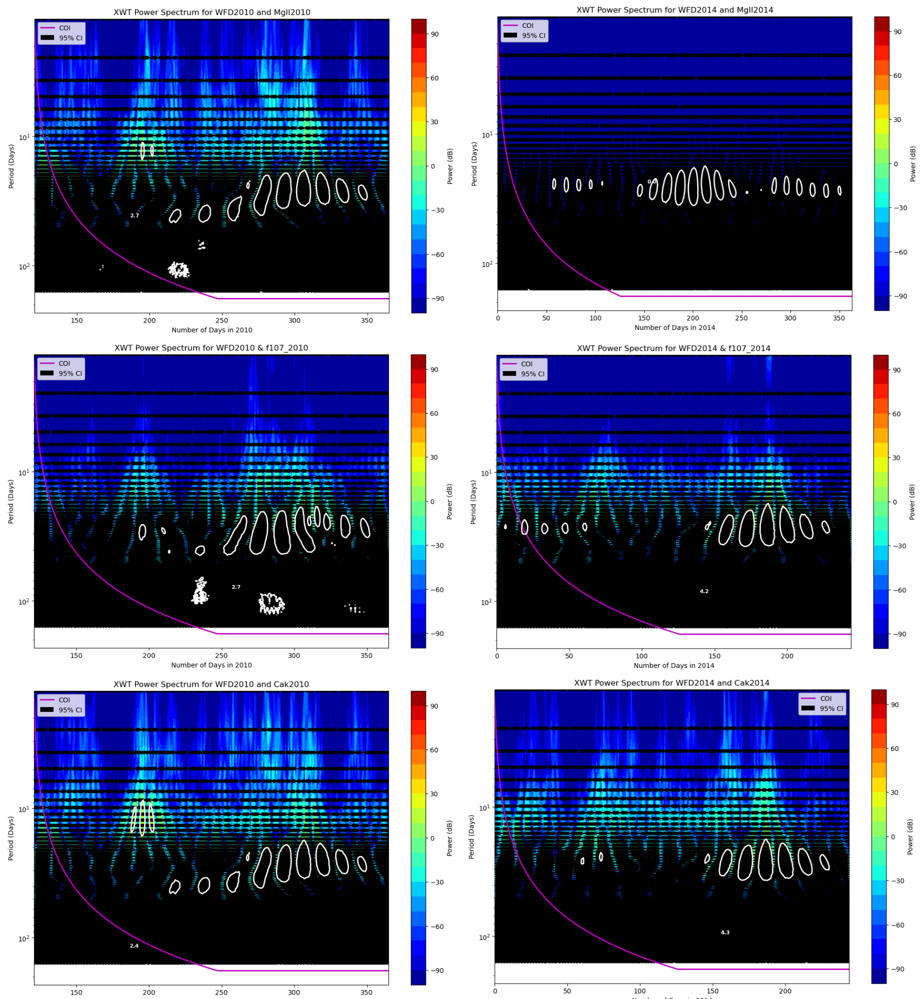

Figure 4.6: XWT for WFD and Solar UV Proxies in 2010 (LHS) and 2014 (RHS)

Figures 4.6 and 4.7 represent XWT between SSI, WFD and solar UV proxies during solar minimum and solar maximum. The figures show the log2-scaled power of the XWT coefficients, representing the strength of common oscillations between the signals over time. The x-axes represent the number of days in 2010 and 2014, while the y-axes represent the period (in days) of the oscillations, displayed on a logarithmic scale (log2). The COI is plotted as a magenta line and it indicates the region where edge effects distort the analysis. Data outside this region should be interpreted with caution or should be ignored, as in this case. The black lines represents the CI while the concentrated white contours represent regions where the power exceeds the 95% CI, indicating significant common oscillations.

Black arrows indicate the phase relationship between the two signals in each diagram:

Black arrows pointing right (or left) indicate in-phase (or anti-phase) oscillations. Upward (or downward) pointing arrows indicate that one signal leads (or lags) the other, by factors clearly seen in Figures 4.8 and 4.9. Bright regions in the plot represent periods and times where both signals exhibit strong, coherent oscillations. The white contour lines enclose regions of significant power, indicating robust common oscillations beyond the expected background noise level. The phase arrows provide insights into the lead-lag relationship between the signals:

Arrows pointing to the right and upward suggest the first signal leads the second signal. While arrows pointing to the left and downward suggest the second signal leads the first signal, in both years. Arrows pointing to the right (0° phase difference) indicate that the two signals are in phase, oscillating together. Arrows pointing to the left (180° phase difference) indicate that the signals are in anti-phase. Arrows pointing up or down (90° or -90° or 270° phase difference) suggest a phase lag or lead of a quarter cycle.

The XWT analysis and the figures reveal how the signals are related in terms of their oscillatory behavior throughout 2010 and 2014.

Synchronized Oscillations are the regions of high power, indicating periods and times where both signals exhibit strong, synchronized oscillations in both years. Significant Periodic(inside the contours) which suggest periods where the relationship between the signals are statistically significant. Lead-Lag Dynamics are Phase arrows that help identify potential causal relationships, with one signal possibly driving or lagging the other at specific periods.

The numbers beside the contours on the plot represent the actual values of the power of the XWT at specific time and period combinations. The numbers indicate the strength of the common oscillatory power between the two signals at a given time and period. Higher values correspond to regions where the signals exhibit strong synchronized oscillations. These values are on a log2 scale. By looking at how these numbers change over time, one can study the evolution of the relationship between the signals throughout the year. And researchers can use these numbers to pinpoint the dominant periods where the two signals exhibit strong correlations.

Overall, the XWT analysis provides a powerful tool for exploring the tempo-

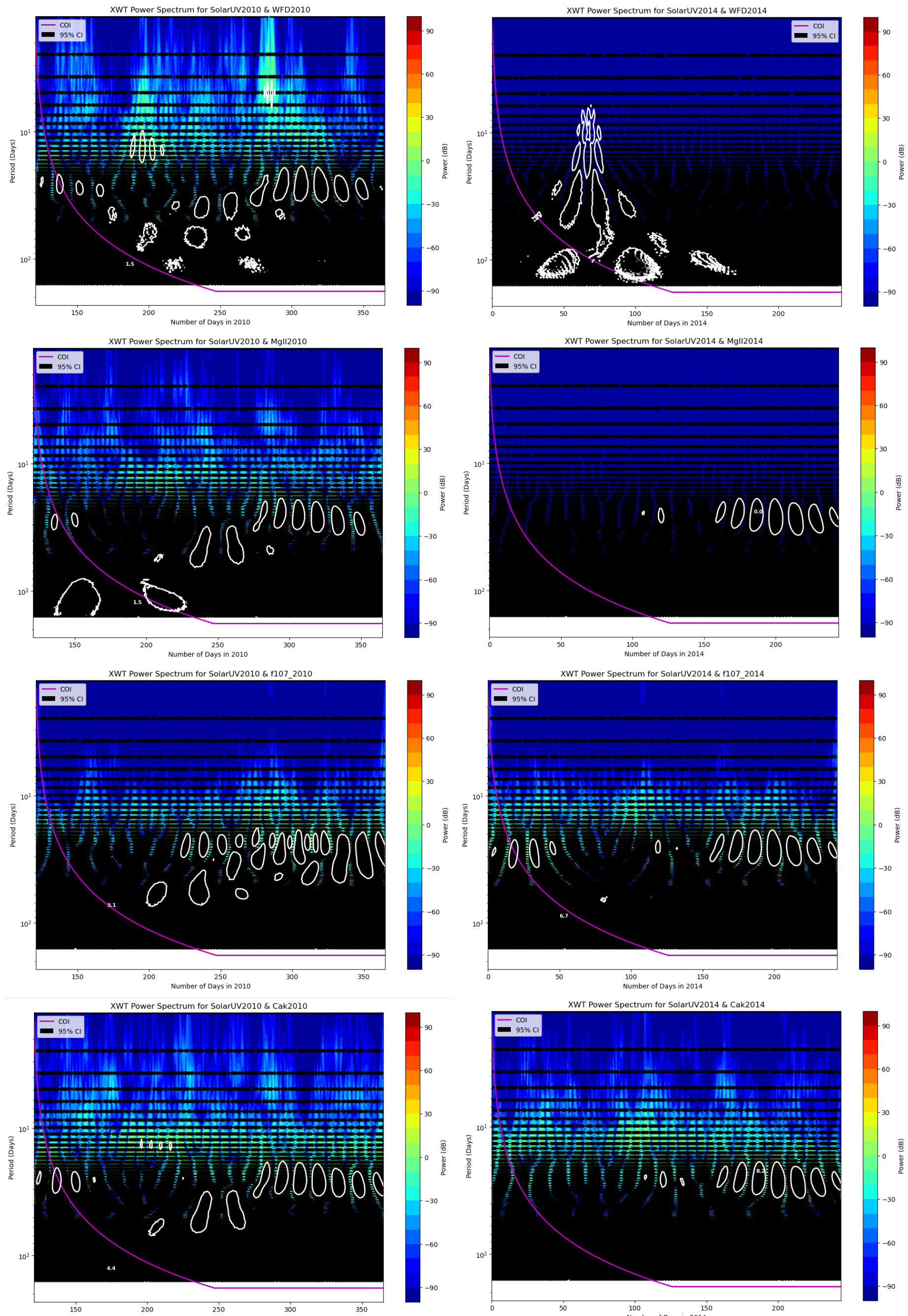

Figure 4.7: XWT for SSI and Solar UV Proxies in 2010 (LHS) and 2014 (RHS)

ral and periodic relationships between the solar ultraviolet and the solar surface flux density , offering insights into their interaction and potential underlying mechanisms. This analysis is crucial for understanding how solar UV variability is influenced by solar surface magnetic flux density.

The first two diagrams of figure 4.7 show significant coherence at periods around 32 days, 64 days, and extending to around 256 days. This indicates that there are common periodicities between SSI and WFD signals at these time scales in both 2010 and 2014. The coherence between SSI and WFD indicates that periods of increased ultraviolet emissions correspond to periods of increased weak flux density. This is consistent with the understanding that higher solar activity (more sunspots and active regions) leads to enhanced UV radiation and increased magnetic flux. The significant periods (32, 64, 128, and 256 days) suggest that the solar activity influencing both UV emissions and weak flux density follows these cycles. Monthly and bi-monthly cycles could be related to the rotation of the Sun, bringing active regions into and out of view. The semi-annual cycle could be related to the solar dynamo processes.

Finally, the XWT power spectrum indicates a strong and significant relationship between SSI and WFD signals across various time scales. This coherence highlights the interconnected nature of different manifestations or changes in solar surface UV irradiance. In solar astrophysics, understanding these relationships helps in predicting space weather impacts, studying the solar cycle, and improving models of solar-terrestrial interactions.

4.3 Correlogram Analysis

This analysis involves identifying signal behaviour, extracting linear and nonlinear properties, compression or expansion into higher or lower dimensions, and recognizing pattern and time of propagation between signal pare.

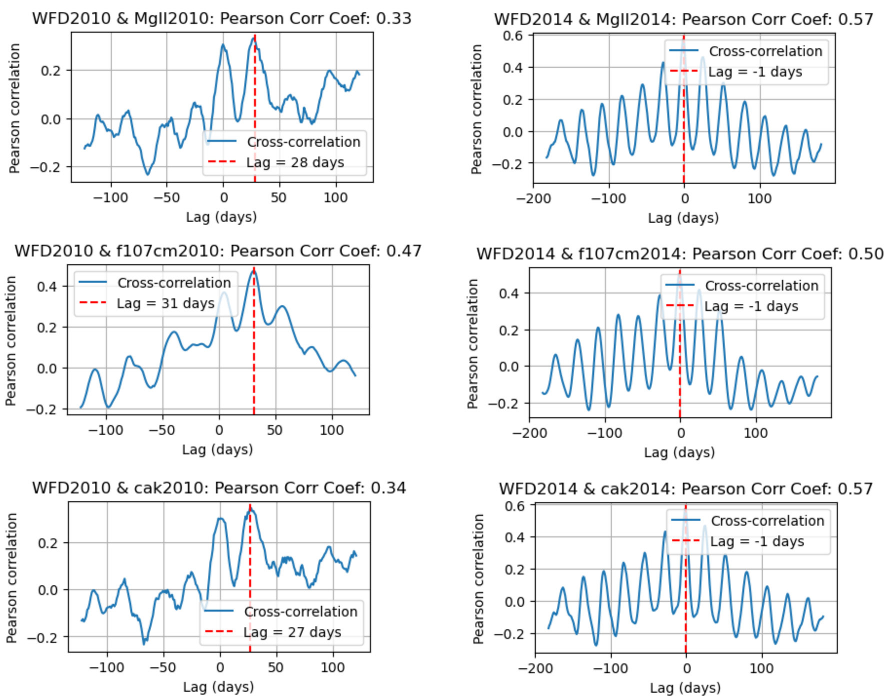

Figure 4.8: Correlogram Analysis for WFD and Solar UV Proxies in 2010 (LHS) and 2014 (RHS)

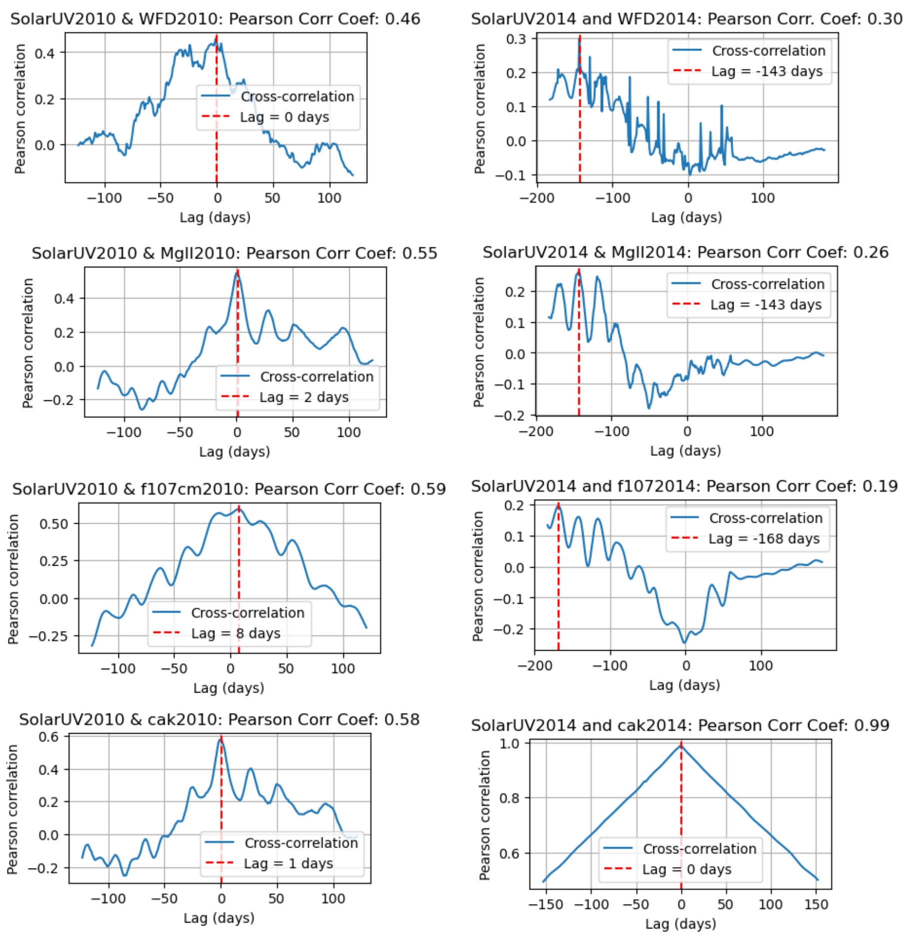

Figure 4.9: Correlogram Analysis for SSI and Solar UV Proxies in 2010 (LHS) and 2014 (RHS)

Figures 4.8 and 4.9 provide the visualization of the calculated Pearson correlation coefficients, lag days and cross-correlation between the signals for 2010 and 2014. The resulting cross-correlation values are normalized by the product of the standard deviations of the two signals.

The lag time is determined by finding the index of the maximum correlation value and adjusting it to center the lag. The maximum correlation value is extracted as the Pearson correlation coefficient. The cross-correlation values are plotted against the lag (in days). A vertical red dashed line indicates the lag time where the correlation is highest. The plot is labeled and includes a legend to clarify the lag time and the Pearson correlation coefficient.

X-axes (Lag in Days): This represents the lag between the two signals, ranging from negative to positive values. A negative lag means the second signal is leading the first signal, while a positive lag means vise versa. Y-axes (Pearson Correlation): This shows the Pearson correlation coefficients, which measures the linear relationships between the two signals at different lags. Cross-Correlation Curve: The curve indicates how the correlation between signals changes with different lags. Red Dashed Line: This line marks the lag time where the correlation is highest.

Peak Correlation: The peak of the cross-correlation curve represents the lag time where signals are most strongly correlated. The height of this peak gives the Pearson correlation coefficient at this lag. Lag Time: The position of the peak (indicated by the red dashed line) tells us the number of days by which one signal leads or lags the other.

A high Pearson correlation coefficient at the peak suggests that the signals are positively correlated at the identified lag time. The lag time indicates the temporal relationship between the signals. For example, if the first signal leads the second signal by a few days, it might suggest that changes in the first signal precede changes in the second signal, possibly due to some atmospheric or solar processes that influence both parameters. The magnitude of the correlation coefficient provides a measure of the strength of the relationship, while the direction (positive or negative) indicates whether the relationship is direct or inverse.

earson Corr Coef: 0.30 and Lag: -143 days Shows a weaker correlation with WFD leading Solar UV by approximately 143 days. This suggests a delayed response of Solar UV to changes in WFD in 2014.

SSI-MgII WITH Pearson Corr Coef: 0.55 AND Lag: 2 days indicates moderate to strong positive correlation with a slight lag of 2 days, indicating that Solar UV is followed by MgII variations shortly in 2010.In figure 4.9. SSI-WFD with Pearson Corr Coef of 0.46 and Lag of 0 days indicates a moderate positive correlation without any significant lag. This implies that the SSI and WFD signals in 2010 vary simultaneously.

While SSI-WFD with P

SSI-MgII with Pearson Corr Coef: 0.2 and Lag: -143 days indicates weaker correlation with MgII leading SSI by about 143 days, indicating a delayed response in 2014 similar to WFD, in the same here.

SSI-f10.7 with Pearson Corr Coef: 0.59 and Lag: 8 days Shows a stronger correlation with Solar UV following the 10.7 cm radio flux (f107cm) by about 8 days, suggesting UV irradiance reacts to changes in solar radio flux within a short delay in 2010.

SSI-f10.7 with Pearson Corr Coef: 0.19 and Lag: -168 days indicates a weak correlation with f10.7 leading Solar UV by 168 days, showing a substantial delayed response in 2014.

SSI-CaK with Pearson Corr Coef: 0.58 and Lag: 1 day represents a strong positive correlation with a minimal lag, suggesting that the Solar UV response to changes in CaK is nearly immediate in 2010

SSI-CaK with Pearson Corr Coef: 0.99 and Lag: 0 days Shows an almost perfect correlation without lag, indicating a direct and synchronous relationship between Solar UV and Ca II K line signals in 2014.

The correlations in 2010 generally show strong and immediate relationships, especially between Solar UV and other proxies like MgII, f10.7, and CaK, indicating that variations in solar ultraviolet irradiance closely track changes in these proxies during this period.

The weaker and more delayed correlations in 2014, particularly with WFD, MgII, and f10.7, suggest a change in the solar activity dynamics. The lead-lag relationships imply that proxies such as WFD and MgII might anticipate changes in Solar UV, potentially due to shifts in solar activity patterns or the influence of different solar phenomena.

MgII, f107cm, and CaK are well-known indicators of solar activity. Their varying correlation strengths and lags with Solar UV across different years provide insights into the changing nature of solar emissions and activity cycles.

The almost perfect correlation between Solar UV and CaK in 2014 underscores the strong linkage between solar UV emissions and chromospheric activity, as Ca II K lines are sensitive to such changes.

The correlogram analysis highlights the dynamic and evolving nature of the relationship between solar ultraviolet irradiance and various solar activity proxies. In 2010, the correlations are stronger and more immediate, while in 2014, they become weaker and more delayed, indicating a potential shift in solar activity mechanisms or external influences affecting these signals. These insights are crucial for understanding solar variability and its impact on the heliosphere and space weather forecasting.

Year	2010			2014		
Names of Signals	WFD vs MgII	WFD vs f10.7	WFD vs CaK	WFD vs MgII	WFD vs f10.7	WFD vs CaK
Pearson Correlation Coefficient	0.3	0.28	0.30	0.45	0.50	0.57
Spearman Correlation Coefficient	0.42	0.46	0.45	0.65	0.60	0.67
Pearson P-value	$2.61Xe^{-06}$	$9.54Xe^{-06}$	$2.07Xe^{-06}$	$1.54Xe^{-29}$	$7.19Xe^{-25}$	$2.99Xe^{-32}$
Spearman P-value	$4.54Xe^{-12}$	$2.82Xe^{-06}$	$1.94Xe^{-13}$	$2.92Xe^{-44}$	$2.23Xe^{-37}$	$5.18Xe^{-48}$
Power Magnitude of XWT (Log2)	2.7	2.7	2.4	-	4.2	4.3

Table 4.1: Pearson correlation coefficients, Spearman correlation coefficients, Pearson P-values, Spearman P-values and XWT power magnitudes for WFD versus Solar UV Proxies in 2010 and 2014.

Year	2010				2014			
Names of Signals	SSI vs MgII	SSI vs f10.7	SSI vs CaK	SSI vs WFD	SSI vs MgII	SSI vs f10.7	SSI vs CaK	SSI vs WFD
Pearson Correlation Coefficient	0.55	0.55	0.57	0.46	0.08	0.12	0.02	0.14
Spearman Correlation Coefficient	0.51	0.64	0.56	0.69	0.21	0.14	0.22	0.23
Pearson P-value	$1.37Xe^{-20}$	$1.04Xe^{-20}$	$1.52Xe^{-20}$	$6.10Xe^{-17}$	0.00	0.04	0.00	0.01
Spearman P-value	$5.96Xe^{-18}$	$1.14Xe^{-29}$	$2.20Xe^{-19}$	$1.42Xe^{-35}$	0.00	0.01	0.00	$7.06Xe^{-05}$
Power Magnitude of XWT (Log2)	1.5	3.1	4.4	1.5	-	6.7	-	-

Table 4.2: Pearson correlation coefficients, Spearman correlation coefficients, Pearson P-values, Spearman P-values and XWT power magnitudes for SSI versus WFD and SSI versus Solar UV Proxies in 2010 and 2014.

4.4 Discussion

The analysis of these signals from 2010 reveals an overall increase in solar activity influenced by WFD, characteristic of the ascending phase of solar cycle 24 as seen in figure 4.1. The different proxies for solar activity, including spectral irradiance, chromospheric indices, and radio flux, all point towards a cohesive rise in solar phenomena. The stability in white-light flare occurrences, despite the general rise in other solar activity indicators, provides an interesting contrast, suggesting that not all solar phenomena increase uniformly during the solar cycle. Understanding these relationships helps solar physicists predict space weather and its potential impacts on Earth's environment and technology.

By studying the relationships between signals on each plot in figure 4.2 and figure 4.3, solar astrophysicists can better understand the dynamics of solar variability and its impacts on the solar-terrestrial environment. In figure 4.2 and figure 4.3, The red lines represent increasing trends, these trend lines provide insights that all the signals are relatively increasing over the years 2010 and 2014 for WFD plots, indicating notable linear events where significant changes are occurring. The strength of this relationships is indicated by Pearson P-value, Spearman P-value, Spearman correlation coefficient, all indicated in tables 4.1 and 4.2.

The observed periodicities around except those between 25 to 35 days in figure 4.4 and figure 4.5 are linked to quasi-periodic variations observed in solar activity, such as the Rieger-type periodicities Gurgenashvili et al. (2021) or rotational modulation of solar emissions. Since WFD is a measure of weak flux densities in solar emissions, its strong correlation and synchronization with solar UV irradiance imply that WFD can be a reliable proxy for studying solar UV variations and overall solar activity.

Finally, the CWT analysis of Solar UV and WFD reveals a strong relationship between these signals, characterized by synchronized periodicities and concurrent high power regions. This indicates that both signals are likely governed by similar solar activity cycles, providing valuable insights into the dynamics of solar emissions and their underlying mechanisms. The similarity in their CWT profiles underscores the interconnected nature of different solar emissions and the utility of WFD as a proxy for solar UV studies.

The XWT analysis in figure 4.6 and figure 4.7 provide a powerful tool for exploring the temporal and periodic relationships between the solar ultraviolet and the solar surface flux density , offering insights into their interaction and potential underlying mechanisms. This analysis is crucial for understanding how solar UV variability is influenced by solar surface magnetic flux density.

The coherence between SSI and WFD indicates that periods of increased ultraviolet emissions correspond to periods of increased weak flux density. This is consistent with the understanding that higher solar activity (more sunspots and active regions) leads to enhanced UV radiation and increased magnetic flux. The significant periods (32, 64, and 256 days) suggest that the solar activity influencing both UV emissions and weak flux density follows these cycles. Monthly and bi-monthly cycles could be related to the rotation of the Sun, bringing active regions into and out of view. The semi-annual cycle could be related to the solar dynamo processes.

Finally, the XWT power spectrum indicates a strong and significant relationship between SSI and WFD signals across various time scales. This coherence highlights the interconnected nature of different manifestations of solar activity. In solar astrophysics, understanding these relationships helps in predicting space weather impacts, studying the solar cycle, and improving models of solar-terrestrial interactions.

In figure 4.8 and figure 4.9, SSI-WFD with Pearson Corr Coef of 0.46 and Lag of 0 days indicate a moderate positive correlation without any significant lag. This implies that the SSI and WFD signals in 2010 vary simultaneously. While SSI-WFD with Pearson Corr Coef: 0.30 and Lag: -143 days Shows a weaker correlation with WFD leading Solar UV by approximately 143 days. This suggests a delayed response of Solar UV to changes in WFD in 2014. SSI-MgII WITH Pearson Corr Coef: 0.55 AND Lag: 2 days indicates mod- erate to strong positive correlation with a slight lag of 2 days, indicating that Solar UV is followed by MgII variations shortly in 2010. SSI-MgII with Pearson Corr Coef: 0.2 and Lag: -143 days indicates weaker correlation with MgII leading SSI by about 143 days, indicating a delayed re- sponse in 2014 similar to WFD, in the same here. SSI-f10.7 with Pearson Corr Coef: 0.59 and Lag: 8 days Shows a stronger correlation with Solar UV following the 10.7 cm radio flux (f107cm) by about 8 days, suggesting UV irradiance reacts to changes in solar radio flux within a short delay in 2010. SSI-f10.7 with Pearson Corr Coef: 0.19 and Lag: -168 days indicates a weak correlation with f10.7 leading Solar UV by 168 days, showing a substantial delayed response in 2014.

Chapter 5

Conclusion and Recommendation

5.1 Conclusion

Generally, the solar activity proxies (MgII, f10.7 and Cak) showed a linear relation with SSI and with the developed time series datasets of solar surface magnetic flux density with a range from 10G to 800G in both 2010 and 2014. Furthermore, there was a significant relationship between SSI and WFD in 2010 than in 2014, indicating that solar surface magnetic flux density had an influence in the solar UV variability during the solar minimum (2010) and solar maximum (2014).

Moreover, the highlights of the correlogram analyses indicates a potential shift in solar activity mechanisms and signifies other external influences affecting solar activity.

5.2 Recommendations

5.2.1 Further Analysis of Magnetic Energy Balance

Future research can be focused on studying the Magnetic Energy Balance in the Quiet Sun. This will help us to understand how the magnetic fields in the quiet solar photosphere store and transfer its energy to the solar upper atmospheric layers.

5.2.2 Extended Time Series Analysis

Future research should expand the time series analysis to include data to solar cycles. This will provide a more comprehensive understanding of the solar activity patterns and their variability over longer time periods.

5.2.3 Investigation of External Influences

Future research should explore other external influences affecting solar activity, as suggested by the potential shift in solar activity mechanisms identified in the correlogram analyses in this project. This could include studying the impact of cosmic rays, interstellar medium, and planetary alignments on the solar activity.

5.2.4 Improvement of Solar Activity Models

Future research should enhance solar activity models by incorporating the findings from this study, especially the relationship between solar surface magnetic flux density and solar UV variability. This will improve predictions of space weather, its impacts and solar-terrestrial interactions.

5.2.5 Cross-Disciplinary Studies

Future research should encourage cross-disciplinary studies involving astrophysics, climate science and space weather forecasting to better understand the implications of solar UV variability on our Earth's climate systems and the space weather phenomena.

5.3 Future Work

In the future, we're planning to study the Magnetic Energy Balance in the Quiet Sun, in other to understand how magnetic fields in the quiet solar photosphere store and transfer energy to the upper atmospheric layers of the Sun.

Bibliography

Addison, P. S. (2017). *The illustrated wavelet transform handbook: introductory theory and applications in science, engineering, medicine and finance*. CRC press.

Ansor, N., Johari, N., Hamidi, Z., and Shariff, N. (2023). Solar activity-climate relations during solar cycle 24. In *IOP Conference Series: Earth and Environmental Science*, volume 1151, page 012022. IOP Publishing.

Archontis, V. and Syntelis, P. (2019). The emergence of magnetic flux and its role on the onset of solar dynamic events. *Philosophical Transactions of the Royal Society A*, 377(2148):20180387.

Arsen'yev, S. A., Eppelbaum, L. V., and Ermakov, N. N. (2019). Dangerous atmospheric events: a new physical mathematical approach. *ANAS Trans. Earth Sci*, 1:11–24.

Babcock, H. (1961). The topology of the sun's magnetic field and the 22-year cycle. *Astrophysical Journal, vol. 133, p. 572*, 133:572.

Babcock, H. D. (1959). The sun's polar magnetic field. *Astrophysical Journal, vol. 130, p. 364*, 130:364.

Babcock, H. W. and Babcock, H. D. (1955). The sun's magnetic field, 1952-1954. *Astrophysical Journal, vol. 121, p. 349*, 121:349.

Balmaceda, L. A., Solanki, S., Krivova, N., and Foster, S. (2009). A homogeneous database of sunspot areas covering more than 130 years. *Journal of Geophysical Research: Space Physics*, 114(A7).

Basu, S., Chaplin, W. J., Elsworth, Y., New, R., and Serenelli, A. M. (2009). Fresh insights on the structure of the solar core. *The Astrophysical Journal*, 699(2):1403.

Biswas, A., Karak, B. B., Usoskin, I., and Weisshaar, E. (2023). Long-term modulation of solar cycles. *Space Science Reviews*, 219(3):19.

Bonanno, A., Schlattl, H., and Paternò, L. (2002). The age of the sun and the relativistic corrections in the eos. *Astronomy & Astrophysics*, 390(3):1115–1118.

Brueckner, G., Edlow, K., Floyd IV, L., Lean, J., and VanHoosier, M. (1993). The solar ultraviolet spectral irradiance monitor (susim) experiment on board the upper atmosphere research satellite (uars). *Journal of Geophysical Research: Atmospheres*, 98(D6):10695–10711.

Canter, L. W. and Wood, C. (1996). Environmental impact assessment.

Chapman, G. and Sheeley Jr, N. (1968). The photospheric network. *Solar Physics, Volume 5, Issue 4, pp. 442-461*, 5:442–461.

Cheung, C. M. M. (2006). Magnetic flux emergence in the solar photosphere.

Cheung, M. and Isobe, H. (2014). Flux emergence (theory). *Living Reviews in Solar Physics*, 11(1):1–128.

Coddington, O., Lean, J., Pilewskie, P., Snow, M., Richard, E., Kopp, G., Lindholm, C., Deland, M., Marchenko, S., Haberreiter, M., et al. (2019). Solar irradiance variability: comparisons of models and measurements. *Earth and Space Science*, 6(12):2525–2555.

DeLand, M. T., Bhartia, P. K., Kramarova, N., and Chen, Z. (2020). Omps lp observations of psc variability during the nh 2019–2020 season. *Geophysical Research Letters*, 47(20):e2020GL090216.

DeLand, M. T. and Cebula, R. P. (2008). Creation of a composite solar ultraviolet irradiance data set. *Journal of Geophysical Research: Space Physics*, 113(A11).

DeLand, M. T., Kopp, G., and Considine, D. B. (2019). Overview of the nasa solar irradiance science team (sist) program special section. *Earth and Space Science*, 6(12):2229–2231.

Dewitte, S. and Nevens, S. (2016). The total solar irradiance climate data record. *The Astrophysical Journal*, 830(1):25.

Domingo, V., Ermolli, I., Fox, P., Fröhlich, C., Haberreiter, M., Krivova, N., Kopp, G., Schmutz, W., Solanki, S., Spruit, H., et al. (2009). Solar surface magnetism and irradiance on time scales from days to the 11-year cycle. *Space Science Reviews*, 145:337–380.

Eddy, J. A. (1976). The maunder minimum: The reign of louis xiv appears to have been a time of real anomaly in the behavior of the sun. *Science*, 192(4245):1189–1202.

Eppelbaum, L. (2019). *Geophysical potential fields: geological and environmental applications*. Elsevier.

Erdmann, W., Kmita, H., Kosicki, J. Z., and Kaczmarek, Ł. (2021). How the geomagnetic field influences life on earth–an integrated approach to geomagnetobiology. *Origins of Life and Evolution of Biospheres*, 51(3):231–257.

Fan, Y. (2009). The emergence of a twisted flux tube into the solar atmosphere: sunspot rotations and the formation of a coronal flux rope. *The Astrophysical Journal*, 697(2):1529.

Fligge, M., Solanki, S., and Unruh, Y. (2000). Modelling irradiance variations from the surface distribution of the solar magnetic field. *Astronomy and Astrophysics, v. 353, p. 380-388 (2000)*, 353:380–388.

Floyd, D. J., Kukula, M. J., Dunlop, J. S., McLure, R. J., Miller, L., Percival, W. J., Baum, S. A., and O'Dea, C. P. (2004). The host galaxies of luminous quasars. *Monthly Notices of the Royal Astronomical Society*, 355(1):196–220.

Fraknoi, A., Morrison, D., and Wolff, S. C. (2018). Astronomy (openstax).

Fröhlich, C. (2000). Observations of irradiance variations. *Space Science Reviews*, 94(1):15–24.

Fröhlich, C. and Lean, J. (2004). Solar radiative output and its variability: evidence and mechanisms. *The Astronomy and Astrophysics Review*, 12(4):273–320.

García, R., Magerle, R., and Perez, R. (2007). Nanoscale compositional mapping with gentle forces. *Nature materials*, 6(6):405–411.

Ghizaru, M., Charbonneau, P., and Smolarkiewicz, P. K. (2010). Magnetic cycles in global large-eddy simulations of solar convection. *The Astrophysical Journal Letters*, 715(2):L133.

Gilliland, R. L. (1982). Modeling solar variability. *Astrophysical Journal, Part 1, vol. 253, Feb. 1, 1982, p. 399-405.*, 253:399–405.

Gizon, L. and Birch, A. C. (2005). Local helioseismology. *Living Reviews in Solar Physics*, 2:1–131.

Gordon, C., Cooper, C., Senior, C. A., Banks, H., Gregory, J. M., Johns, T. C., Mitchell, J. F., and Wood, R. A. (2000). The simulation of sst, sea ice extents and ocean heat transports in a version of the hadley centre coupled model without flux adjustments. *Climate dynamics*, 16:147–168.

Gray, L. J., Beer, J., Geller, M., Haigh, J. D., Lockwood, M., Matthes, K., Cubasch, U., Fleitmann, D., Harrison, G., Hood, L., et al. (2010). Solar influences on climate. *Reviews of Geophysics*, 48(4).

Grinsted, A., Moore, J. C., and Jevrejeva, S. (2004). Application of the cross wavelet transform and wavelet coherence to geophysical time series. *Nonlinear processes in geophysics*, 11(5/6):561–566.

Gröbner, J. (2012). Ultraviolet radiation: distribution and variability. In *Environmental Toxicology: Selected Entries from the Encyclopedia of Sustainability Science and Technology*, pages 595–607. Springer.

Guharay, A., Batista, P. P., Buriti, R. A., and Schuch, N. J. (2020). Signature of the 27-day oscillation in the mlt tides and its relation with solar radiation at low latitudes. *Earth, Planets and Space*, 72:1–10.

Gurgenashvili, E., Zaqarashvili, T., Kukhianidze, V., Reiners, A., Oliver, R., Lanza, A. F., and Reinhold, T. (2021). Rieger-type periodicity in the total irradiance of the sun as a star during solar cycles 23–24. *Astronomy & Astrophysics*, 653:A146.

Haberreiter, M., Schöll, M., Dudok de Wit, T., Kretzschmar, M., Misios, S., Tourpali, K., and Schmutz, W. (2017). A new observational solar irradiance composite. *Journal of Geophysical Research: Space Physics*, 122(6):5910–5930.

Hale, G. E. (1908). 16. on the probable existence of a magnetic field in sun-spots. *Astrophysical Journal*, 28:315–343.

Hall, J. C. (2008). Stellar chromospheric activity. *Living Reviews in Solar Physics*, 5(1):1–53.

Hathaway, D. H. (2015). The solar cycle. *Living reviews in solar physics*, 12(1):4.

Hathaway, D. H. and Rightmire, L. (2010). Variations in the sun's meridional flow over a solar cycle. *Science*, 327(5971):1350–1352.

Hayakawa, H., Carrasco, V. M., Aparicio, A. J., Villalba Álvarez, J., and Vaquero, J. M. (2024). An overview of sunspot observations in the early maunder minimum: 1645–1659. *Monthly Notices of the Royal Astronomical Society*, 528(4):6280–6291.

Heath, D. F. and Schlesinger, B. M. (1986). The mg 280-nm doublet as a monitor of changes in solar ultraviolet irradiance. *Journal of Geophysical Research: Atmospheres*, 91(D8):8672–8682.

Howard, R., Sheeley Jr, N., Koomen, M., and Michels, D. (1985). Coronal mass ejections: 1979–1981. *Journal of Geophysical Research: Space Physics*, 90(A9):8173–8191.

Howe, R. (2009). Solar interior rotation and its variation. *Living Reviews in Solar Physics*, 6(1):1–75.

Hudson, H. (1988). Observed variability of the solar luminosity. *IN: Annual review of astronomy and astrophysics. Volume 26 (A89-14601 03-90). Palo Alto, CA, Annual Reviews, Inc., 1988, p. 473-507. NASA-supported research.*, 26:473–507.

Imbriani, G., Costantini, H., Formicola, A., Bemmerer, D., Bonetti, R., Broggini, C., Corvisiero, P., Cruz, J., Fülöp, Z., Gervino, G., et al. (2004). The bottleneck of cno burning and the age of globular clusters. *Astronomy & Astrophysics*, 420(2):625–629.

Kakuwa, J. and Ueno, S. (2022). Investigation of the long-term variation of solar ca ii k intensity. ii. reconstruction of solar uv irradiance. *The Astrophysical Journal*, 928(1):97.

Karak, B. B. (2023). Models for the long-term variations of solar activity. *Living Reviews in Solar Physics*, 20(1):3.

Kodera, K. (2004). Solar influence on the indian ocean monsoon through dynamical processes. *Geophysical Research Letters*, 31(24).

Krivova, N., Solanki, S., and Floyd, L. (2006). Reconstruction of solar uv irradiance in cycle 23. *Astronomy & Astrophysics*, 452(2):631–639.

Krivova, N., Solanki, S., Hofer, B., Wu, C.-J., Usoskin, I., and Cameron, R. (2021). Modelling the evolution of the sun's open and total magnetic flux. *Astronomy & Astrophysics*, 650:A70.

Kutsenko, A. and Abramenko, V. (2016). Using sdo/hmi magnetograms as a source of the solar mean magnetic field data. *Solar Physics*, 291:1613–1623.

Lean, J. (2000). Evolution of the sun's spectral irradiance since the maunder minimum. *Geophysical research letters*, 27(16):2425–2428.

Lean, J., Coddington, O., Marchenko, S., Machol, J., DeLand, M., and Kopp, G. (2020). Solar irradiance variability: Modeling the measurements. *Earth and Space Science*, 7(8):e2019EA000645.

Lean, J., Rottman, G., Harder, J., and Kopp, G. (2005). Sorce contributions to new understanding of global change and solar variability. *The Solar Radiation and Climate Experiment (SORCE) Mission Description and Early Results*, pages 27–53.

Lean, J., Woods, T., Eparvier, F., Meier, R., Strickland, D., Correira, J., and Evans, J. (2011). Solar extreme ultraviolet irradiance: Present, past, and future. *Journal of Geophysical Research: Space Physics*, 116(A1).

Lilensten, J., Dudok de Wit, T., Amblard, P.-O., Aboudarham, J., Auchère, F., and Kretzschmar, M. (2007). Recommendation for a set of solar euv lines to be monitored for aeronomy applications. In *Annales Geophysicae*, volume 25, pages 1299–1310. Copernicus Publications Göttingen, Germany.

Lkhagvadorj, M. (2023). Propagation of interplanetary shocks in the heliosphere. *arXiv preprint arXiv:2307.03328*.

Lockwood, M. and Stamper, R. (1999). Long-term drift of the coronal source magnetic flux and the total solar irradiance. *Geophysical research letters*, 26(16):2461–2464.

Manchester, R. N., Fan, G., Lyne, A., Kaspi, V., and Crawford, F. (2006). Discovery of 14 radio pulsars in a survey of the magellanic clouds. *The Astrophysical Journal*, 649(1):235.

Marchenko, S. V., Lean, J. L., and DeLand, M. T. (2022). Relationship between total solar irradiance and magnetic flux during solar minima. *The Astrophysical Journal*, 936(2):158.

Matthes, K., Funke, B., Andersson, M. E., Barnard, L., Beer, J., Charbonneau, P., Clilverd, M. A., Dudok de Wit, T., Haberreiter, M., Hendry, A., et al. (2017). Solar forcing for cmip6 (v3. 2). *Geoscientific Model Development*, 10(6):2247–2302.

Merry, R. (2005). Wavelet theory and applications: a literature study.

Mestel, L. and Spruit, H. (1987). On magnetic braking of late-type stars. *Monthly Notices of the Royal Astronomical Society*, 226(1):57–66.

Moldwin, M. (2000). How big is our sun? *The Physics Teacher*, 38(115).

Moss, R. H., Babiker, M., Brinkman, S., Calvo, E., Carter, T., Edmonds, J. A., Elgizouli, I., Emori, S., Lin, E., Hibbard, K., et al. (2008). Towards new scenarios for analysis of emissions, climate change, impacts, and response strategies.

Muñoz-Jaramillo, A., Dasi-Espuig, M., Balmaceda, L. A., and DeLuca, E. E. (2013). Solar cycle propagation, memory, and prediction: insights from a century of magnetic proxies. *The Astrophysical Journal Letters*, 767(2):L25.

Pariat, E., Aulanier, G., Schmieder, B., Georgoulis, M. K., Rust, D., and Bernasconi, P. N. (2004). Resistive emergence of undulatory flux tubes. *The Astrophysical Journal*, 614(2):1099.

Pauluhn, A. and Solanki, S. (2002). Surface magnetic fields and uv radiance of the quiet sun. In *SOLMAG 2002. Proceedings of the Magnetic Coupling of the Solar Atmosphere Euroconference*, volume 505, pages 521–524.

Pauluhn, A. and Solanki, S. (2003). Dependence of uv radiance of the quiet sun on the solar cycle: Surface magnetic fields as the cause. *Astronomy & Astrophysics*, 407(1):359–367.

Peterson, B. M., Wanders, I., Horne, K., Collier, S., Alexander, T., Kaspi, S., and Maoz, D. (1998). On uncertainties in cross-correlation lags and the reality of wavelength-dependent continuum lags in active galactic nuclei. *Publications of the Astronomical Society of the Pacific*, 110(748):660.

Petrovay, K. (2020). Solar cycle prediction. *Living Reviews in Solar Physics*, 17(1):2.

Pietrow, A., Cretignier, M., Druett, M., Alvarado-Gómez, J., Hofmeister, S., Verma, M., Kamlah, R., Baratella, M., Amazo-Gómez, E., Kontogiannis, I., et al. (2024). A comparative study of two x2. 2 and x9. 3 solar flares observed with harps-n-reconciling sun-as-a-star spectroscopy and high-spatial resolution solar observations in the context of the solar-stellar connection. *Astronomy & Astrophysics*, 682:A46.

Rempel, M. and Cheung, M. (2014). Numerical simulations of active region scale flux emergence: from spot formation to decay. *The Astrophysical Journal*, 785(2):90.

Ribes, J. and Nesme-Ribes, E. (1993). The solar sunspot cycle in the maunder minimum ad1645 to ad1715. *Astronomy and Astrophysics, Vol. 276, p. 549 (1993)*, 276:549.

Robitaille, P.-M. (2013). Commentary on the radius of the sun: Optical illusion or manifestation of a real surface. *Progr. Phys*, 2:L5–L6.

Rottman, G. J., Woods, T. N., and Sparn, T. P. (1993). Solar-stellar irradiance comparison experiment 1: 1. instrument design and operation. *Journal of Geophysical Research: Atmospheres*, 98(D6):10667–10677.

Schmieder, B. and Pariat, E. (2007). Magnetic flux emergence. *Scholarpedia*, 2(12):4335.

Schou, J., Scherrer, P. H., Bush, R. I., Wachter, R., Couvidat, S., Rabello-Soares, M. C., Bogart, R. S., Hoeksema, J., Liu, Y., Duvall, T., et al. (2012). Design and ground calibration of the helioseismic and magnetic imager (hmi) instrument on the solar dynamics observatory (sdo). *Solar Physics*, 275:229–259.

Shibata, K., Ishido, Y., Acton, L., Strong, K., Hirayama, T., Uchida, Y., McAllister, A., Matsumoto, R., Tsuneta, S., Shimizu, T., et al. (1993). Observations of x-ray jets using yohkoh soft x-ray telescope. In *International Astronomical Union Colloquium*, volume 141, pages 343–346. Cambridge University Press.

Shukure, N., Tessema, S., and Gopalswamy, N. (2021a). On the connection between solar surface magnetic flux and the total solar irradiance. *The Astrophysical Journal*, 907(1):39.

Shukure, N., Tessema, S., and Gopalswamy, N. (2021b). Total solar irradiance variability on the evolutionary timescale and its impact on the earth's mean surface temperature. *The Astrophysical Journal*, 917(2):86.

Simon, P., Rottman, G., White, O., and Knapp, B. (1988). Short term variability between 120 and 300 nm from sme observations.

Skupin, J., Noel, S., Wuttke, M. W., Gottwald, M., Bovensmann, H., Weber, M., and Burrows, J. P. (2005). Sciamachy solar irradiance observation in the spectral range from 240 to 2380 nm. *Advances in space research*, 35(3):370–375.

Snow, M., McClintock, W. E., Woods, T. N., and Elliott, J. P. (2022). Solar-stellar irradiance comparison experiment ii (solstice ii): end-of-mission validation of the solstice technique. *Solar Physics*, 297(5):55.

Snow, M., Weber, M., Machol, J., Viereck, R., and Richard, E. (2014). Comparison of magnesium ii core-to-wing ratio observations during solar minimum 23/24. *Journal of Space Weather and Space Climate*, 4:A04.

Solanki, S., Barthol, P., Danilovic, S., Feller, A., Gandorfer, A., Hirzberger, J., Riethmüller, T., Schüssler, M., Bonet, J., Pillet, V. M., et al. (2010). Sunrise: instrument, mission, data, and first results. *The Astrophysical Journal Letters*, 723(2):L127.

Solanki, S. and Fligge, M. (1999). A reconstruction of total solar irradiance since 1700. *Geophysical Research Letters*, 26(16):2465–2468.

Solanki, S., Schüssler, M., and Fligge, M. (2000). Evolution of the sun's large-scale magnetic field since the maunder minimum. *Nature*, 408(6811):445–447.

Solanki, S. K., Inhester, B., and Schüssler, M. (2006). The solar magnetic field. *Reports on Progress in Physics*, 69(3):563.

Solanki, S. K., Krivova, N. A., and Haigh, J. D. (2013). Solar irradiance variability and climate. *Annual Review of Astronomy and Astrophysics*, 51:311–351.

Solanki, S. K., Usoskin, I. G., Kromer, B., Schüssler, M., and Beer, J. (2004). Unusual activity of the sun during recent decades compared to the previous 11,000 years. *Nature*, 431(7012):1084–1087.

Stenflo, J. O. (2017). History of solar magnetic fields since george ellery hale. *Space Science Reviews*, 210:5–35.

Subbaraya, B. (1998). Solar uv variability.

Tapping, K. (1987). Recent solar radio astronomy at centimeter wavelengths: The temporal variability of the 10.7-cm flux. *Journal of Geophysical Research: Atmospheres*, 92(D1):829–838.

Tapping, K. (2013). The 10.7 cm solar radio flux (f10. 7). *Space weather*, 11(7):394–406.

Temmer, M. (2021). Space weather: The solar perspective: An update to schwenn (2006). *Living Reviews in Solar Physics*, 18(1):4.

Thiemann, E., Harder, J., Woods, T., Snow, M., Klapetzky, M., Triplett, M., Sims, A., Penton, S., and Furst, M. (2023). Solar irradiance spectra from the compact solstice (csol) experiment: Instrument design, fuv calibration, measurements, and comparison of the 2018 rocket flight. *Solar Physics*, 298(2):17.

Thompson, M. J., Christensen-Dalsgaard, J., Miesch, M. S., and Toomre, J. (2003). The internal rotation of the sun. *Annual Review of Astronomy and Astrophysics*, 41(1):599–643.

Tian, H., McIntosh, S. W., De Pontieu, B., Martínez-Sykora, J., Sechler, M., and Wang, X. (2011). Two components of the solar coronal emission revealed by extreme-ultraviolet spectroscopic observations. *The Astrophysical Journal*, 738(1):18.

Toriumi, S., Miyagoshi, T., Yokoyama, T., Isobe, H., and Shibata, K. (2011). Dependence of the magnetic energy of solar active regions on the twist intensity of the initial flux tubes. *Publications of the Astronomical Society of Japan*, 63(2):407–415.

Torrence, C. and Compo, G. P. (1998). A practical guide to wavelet analysis. *Bulletin of the American Meteorological society*, 79(1):61–78.

Tortosa-Andreu, A. and Moreno-Insertis, F. (2009). Magnetic flux emergence into the solar photosphere and chromosphere. *Astronomy & Astrophysics*, 507(2):949–967.

Tsuneta, S., Ichimoto, K., Katsukawa, Y., Lites, B. W., Matsuzaki, K., Nagata, S., Suárez, D. O., Shimizu, T., Shimojo, M., Shine, R., et al. (2008). The magnetic landscape of the sun's polar region. *The Astrophysical Journal*, 688(2):1374.

Usoskin, I., Koldobskiy, S., Poluianov, S., Raukunen, O., Vainio, R., and Kovaltsov, G. (2023). Consistency of the average flux of solar energetic particles over timescales of years to megayears. *Astronomy & Astrophysics*, 670:L22.

Usoskin, I., Schüssler, M., Solanki, S., and Mursula, K. (2005). Solar activity, cosmic rays, and earth's temperature: A millennium-scale comparison. *Journal of Geophysical Research: Space Physics*, 110(A10).

Usoskin, I. G., Mursula, K., Solanki, S., Schüssler, M., and Alanko, K. (2004). Reconstruction of solar activity for the last millennium using be data. *Astronomy & Astrophysics*, 413(2):745–751.

Usoskin, I. G., Solanki, S. K., and Kovaltsov, G. A. (2007). Grand minima and maxima of solar activity: new observational constraints. *Astronomy & Astrophysics*, 471(1):301–309.

Vaquero, L. M., Rodero-Merino, L., and Morán, D. (2011). Locking the sky: a survey on iaas cloud security. *Computing*, 91:93–118.

Viereck, R. A. and Puga, L. C. (1999). The noaa mg ii core-to-wing solar index: Construction of a 20-year time series of chromospheric variability from multiple satellites. *Journal of Geophysical Research: Space Physics*, 104(A5):9995–10005.

Woolfson, M. M. (2000). *The origin and evolution of the solar system*. CRC Press.

Worden, J. R., White, O. R., and Woods, T. N. (1998). Evolution of chromospheric structures derived from ca ii k spectroheliograms: implications for solar ultraviolet irradiance variability. *The Astrophysical Journal*, 496(2):998.

Yeo, K. L., Solanki, S. K., and Krivova, N. A. (2020). How faculae and network relate to sunspots, and the implications for solar and stellar brightness variations. *Astronomy & Astrophysics*, 639:A139.

Zolotova, N. and Ponyavin, D. (2016). How deep was the maunder minimum? *Solar Physics*, 291:2869–2890.

Declaration

I hereby declare that this MSc thesis is my original work and has not been presented for a degree in any other universities, and that all sources of material used for the project have been duly acknowledged.

Name: Mbonteh Roland Ndunge

Signature: ____________________

This research thesis has been submitted for evaluation with the approval of a university advisor.

Name: Dr. Negessa Tilahun S.

Signature: ____________________

Place and date of submission:

Addis Ababa University
College of Natural and Computational Sciences
Department of Physics
July 30, 2024